



## Available online at www.sciencedirect.com

# **ScienceDirect**

Geochimica et Cosmochimica Acta

Geochimica et Cosmochimica Acta 314 (2021) 313-333

www.elsevier.com/locate/gca

# Trajectory and timescale of oxygen and clumped isotope equilibration in the dissolved carbonate system under normal and enzymatically-catalyzed conditions at 25 °C

Joji Uchikawa <sup>a,\*</sup>, Sang Chen <sup>b,c,\*</sup>, John M. Eiler <sup>c</sup>, Jess F. Adkins <sup>c</sup>, Richard E. Zeebe <sup>a</sup>

a Department of Oceanography, SOEST, University of Hawaii at Manoa, Honolulu, HI, USA
 b School of Oceanography, Shanghai Jiao Tong University, Shanghai, China
 c Division of Geological and Planetary Sciences, California Institute of Technology, Pasadena, CA, USA

Received 19 February 2021; accepted in revised form 12 August 2021; available online 20 August 2021

#### Abstract

The abundance of  $^{18}O$  isotopes and  $^{13}C$ - $^{18}O$  isotopic "clumps" (measured as  $\delta^{18}O$  and  $\Delta_{47}$ , respectively) in carbonate minerals have been used to infer mineral formation temperatures. An inherent requirement or assumption for these paleothermometers is mineral formation in isotopic equilibrium. Yet, apparent disequilibrium is not uncommon in biogenic and abiogenic carbonates formed in nature and in synthetic carbonates prepared under laboratory settings, as the dissolved carbonate pool (DCP) from which minerals precipitate is often out of  $\delta^{18}O$  and  $\Delta_{47}$  equilibrium. For this, a complete understanding of both equilibrium and kinetics of isotopic partitioning and <sup>13</sup>C-<sup>18</sup>O clumping in DCP is crucial. To this end, we analyzed  $\Delta_{47}$  of inorganic BaCO<sub>3</sub> samples from Uchikawa and Zeebe (2012) (denoted as UZ12), which were quantitatively precipitated from NaHCO<sub>3</sub> solutions at various times over the course of isotopic equilibration at 25 °C and pH<sub>NBS</sub> of 8.9. Our data show that, although the timescales for  $\delta^{18}O$  and  $\Delta_{47}$  equilibrium in DCP are relatively similar, their equilibration trajectories are markedly different. As opposed to a simple unidirectional and asymptotic approach toward  $\delta^{18}$ O equilibrium (first-order kinetics),  $\Delta_{47}$  equilibration initially moves away from equilibrium and then changes its course towards equilibrium. This excess  $\Delta_{47}$  disequilibrium is manifested as a characteristic "dip" in the  $\Delta_{47}$  equilibration trajectory, a feature consistent with an earlier study by Staudigel and Swart (2018) (denoted as SS18). From the numerical model of SS18, the non-first-order kinetics for  $\Delta_{47}$  equilibration can be understood as a result of the difference in the exchange rate for oxygen isotopes bound to  $^{12}$ C versus  $^{13}$ C, or an isotope effect of ~25%. We also developed an independent model for the *Ex*change and *Clump*ing of  $^{13}$ C and  $^{18}$ O in DCP (ExClump38 model) to trace the evolution of singly- and doubly-substituted isotopic species (*i.e.*,  $^{13}$ C,  $\delta^{18}$ O and  $\Delta_{47}$ ). The model suggests that the dip in the  $\Delta_{47}$  equilibration trajectory is due largely to kinetic carbon isotope fractionation for hydration and hydroxylation of CO2. We additionally examined the BaCO3 samples prepared from NaHCO3 solutions supplemented with carbonic anhydrase (CA), an enzyme known to facilitate  $\delta^{18}$ O equilibration in DCP by catalyzing  $CO_2$  hydration (UZ12). These samples revealed that, while CA effectively shortens the time required for  $\Delta_{47}$  equilibrium in DCP, the overall pattern and magnitude of the dip in the  $\Delta_{47}$  equilibration trajectory remain unchanged. This suggests no

E-mail addresses: uchikawa@hawaii.edu (J. Uchikawa), sang@sjtu.edu.cn (S. Chen).

<sup>\*</sup> Corresponding authors at: Department of Oceanography, SOEST, University of Hawaii, Honolulu, HI 96822, USA (J. Uchikawa); School of Oceanography, Shanghai Jiao Tong University, Shanghai, China (S. Chen).

additional isotope effects due to the CA enzyme within the tested CA concentrations. With the ExClump38 model, we test various physicochemical scenarios for the timescales and trajectories of isotopic equilibration in DCP and discuss their implications for the  $\Delta_{47}$  paleothermometry.

© 2021 Elsevier Ltd. All rights reserved.

Keywords: Clumped isotopes; Oxygen isotopes; Kinetic isotope effects; Carbonic anhydrase; Isotopic equilibration

#### 1. INTRODUCTION

Urey (1947) and McCrea (1950) argued that stable oxygen isotope ratios ( $\delta^{18}$ O) of carbonate minerals (*e.g.*, CaCO<sub>3</sub>) can be used to infer mineral formation temperatures. Theoretical basis of this classic technique, known as the  $\delta^{18}$ O paleothermometry, is rooted in the temperature-dependence of equilibrium for oxygen isotope exchange between CaCO<sub>3</sub> and H<sub>2</sub>O:

$$CaC^{16}O^{16}O^{16}O + H_2^{18}O \leftrightarrow CaC^{18}O^{16}O^{16}O + H_2^{16}O$$
 (1)

Since their pioneering work, this technique still stands as a powerful tool for paleo-temperature reconstructions in many environmental settings and over various spatiotemporal scales. Yet, there are two major drawbacks with this technique. First, as Eq. (1) implies,  $\delta^{18}$ O values of CaCO<sub>3</sub> depend not only temperature but also on  $\delta^{18}$ O of H<sub>2</sub>O in which mineral precipitation occurs. Second,  $\delta^{18}O$  values of natural biogenic (e.g., coral skeletons and foraminiferal shells) and abiogenic CaCO<sub>3</sub> (e.g., speleothems) are typically, and often strongly, out of isotopic equilibrium (McConnaughey, 1989; Adkins et al., 2003; Spero et al., 1997; Daëron et al., 2011; Riechelmann et al., 2013; Falk et al., 2016). Even more fundamentally, Watkins et al. (2013; 2014) experimentally demonstrated that much of laboratory-grown inorganic CaCO<sub>3</sub> prepared in previous calibration studies (e.g., Kim and O'Neil, 1997; Zhou and Zheng, 2003; Kim et al., 2007; Dietzel et al., 2009) unlikely reflect the true isotopic equilibrium between CaCO3 and H<sub>2</sub>O. The problem is that timescales of CaCO<sub>3</sub> precipitation in laboratory settings (also in nature) typically exceeds the regime of very slow precipitation under which the true isotopic equilibrium can only be achieved. Most synthetic and natural CaCO<sub>3</sub> are hence out of δ<sup>18</sup>O equilibrium, except for very rare cases (e.g., Coplen, 2007; Daëron et al., 2019).

Mineral formation temperatures can be also inferred from the abundance of  $^{13}C^{-18}O$  bonds in CaCO3, as the degree of  $^{13}C^{-18}O$  "clumping" is correlated with temperature (Schauble et al., 2006; Eiler, 2007). This approach known as the clumped isotope ( $\Delta_{47}$ ) paleothermometry is independent of  $\delta^{18}O$  of  $H_2O$ , because it is rooted in the equilibrium of internal  $^{13}C^{-18}O$  bond distribution within CaCO3 itself (Ghosh et al., 2006; Eiler, 2011):

$$\begin{array}{lll} Ca^{13}C^{16}O^{16}O^{16}O \ + \ Ca^{12}C^{18}O^{16}O^{16}O \\ & \leftrightarrow \ Ca^{13}C^{18}O^{16}O^{16}O \ + \ Ca^{12}C^{16}O^{16}O^{16}O \end{array} \tag{2}$$

For over a decade, extensive efforts have been put forth to establish a universal calibration of the  $\Delta_{47}$  paleother-

mometry based on laboratory experiments (Ghosh et al., 2006; Dennis and Schrag, 2010; Zaarur et al., 2013; Tang et al., 2014; Kluge et al., 2015; Kelson et al., 2017; Bonifacie et al., 2017; Levitt et al., 2018). However, several incidents of apparent  $\Delta_{47}$  disequilibrium with respect to those inorganic calibrations have been reported for natural CaCO<sub>3</sub> (Daëron et al., 2011; Saenger et al., 2012; Eagle et al., 2013; Henkes et al., 2013; Kluge et al., 2014; Spooner et al., 2016; Falk et al., 2016). Daëron et al. (2019) recently warned that, as is the case for  $\delta^{18}$ O, most natural CaCO<sub>3</sub> are presumably out of  $\Delta_{47}$  equilibrium, and this may extend to synthetic CaCO<sub>3</sub> prepared in previous laboratory-based calibration studies.

It has been argued that both  $\delta^{18}O$  and  $\Delta_{47}$  disequilibrium in CaCO3 are, at least in part, due to precipitation in the dissolved carbonate system that is not in full  $\delta^{18}$ O and  $\Delta_{47}$  equilibrium (Watkins et al., 2013; Watkins et al., 2014; Tang et al., 2014; Watkins and Hunt, 2015; Devriendt et al., 2017; Daëron et al., 2019). From the latest studies it appears that additional consideration of yet another doubly-substituted species in CaCO3, that is  $Ca^{12}C^{18}O^{18}O^{16}O$  quantified as  $\Delta_{48}$ , could be a powerful tool to shed a new light on and possibly even correct for such kinetically-driven isotopic disequilibrium (Guo and Zhou, 2019; Guo, 2020; Bajnai et al., 2020). However, a critical prerequisite for the community at this stage is to fully understand the equilibrium <sup>18</sup>O partitioning and the degree of <sup>13</sup>C-<sup>18</sup>O clumping in the dissolved carbonate system as well as the kinetics of the respective isotopic equilibrations.

Equilibrium oxygen isotope fractionations between individual dissolved inorganic carbon (DIC) species and H<sub>2</sub>O are well constrained. For instance,  $\delta^{18}O$  of HCO<sub>3</sub> is ~6% higher than  $CO_3^{2-}$  in a fully equilibrated system at 25 °C (Beck et al., 2005; Uchikawa and Zeebe, 2013). Given the pH-dependent DIC speciation (Fig. 1a), isotope mass balance imposes  $\delta^{18}$ O of the sum of DIC species to change systematically with pH (Zeebe and Wolf-Gladrow, 2001; Beck et al., 2005; Zeebe, 2007; Uchikawa and Zeebe, 2013, Fig. 1b). Also note that the system essentially becomes a two-component mass balance at pH > -8, where CO<sub>2(aq)</sub> and H<sub>2</sub>CO<sub>3</sub> contributions to the total DIC are negligible (i.e., [DIC]  $\approx$  [HCO $_3^-$ ] + [CO $_3^2^-$ ]). For such conditions, we will specifically use the term "dissolved carbonate pool (DCP)", where DCP is the sum of  $[HCO_3^-]$  and  $[CO_3^{2-}]$ . Direct exchange of oxygen isotopes between DCP and H<sub>2</sub>O occurs via CO<sub>2</sub> hydration or hydroxylation and their reverse reactions (Zeebe and Wolf-Gladrow, 2001):

$$CO_{2(aq)} + H_2O \underset{k_{-1}}{\overset{k_{+1}}{\rightleftharpoons}} HCO_3^- + H^+$$
 (3)

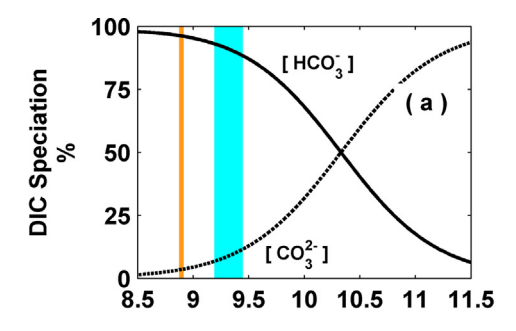
And

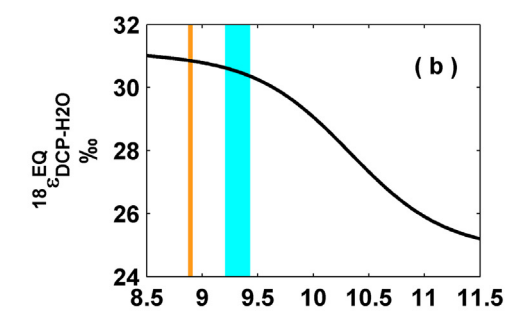
$$CO_{2(aq)} + OH^{-} \underset{k_{-4}}{\overset{k_{+4}}{\rightleftharpoons}} HCO_{3}^{-}$$

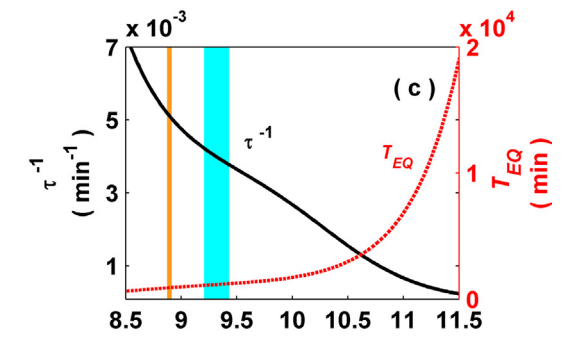
$$\tag{4}$$

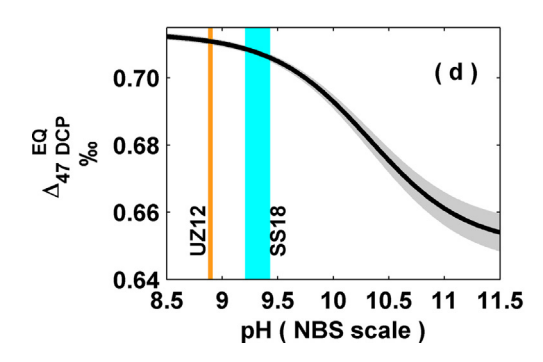
where  $k_{\pm 1}$  and  $k_{\pm 4}$  represent the forward and backward kinetic rate constants. At higher pH,  $\delta^{18}$ O equilibrium takes longer due to a corresponding decrease in [CO<sub>2(aq)</sub>]. The time required for 99% completion of oxygen isotope equilibrium ( $T_{EO}$ ) is given by:

$$T_{EO} = -\ln(0.01) \cdot \tau \tag{5}$$









where the rate constant  $\tau$  can be calculated as a function of pH (as it dictates DIC speciation, see Fig. 1ac) using a set of equilibrium and kinetic rate constants (Usdowski et al., 1991; Uchikawa and Zeebe, 2012) (we abbreviate Uchikawa and Zeebe (2012) as "UZ12" hereafter). With  $\tau$ , the time-course of  $\delta^{18}O$  equilibration can be modeled as:

$$\delta^{18} O_{DCP}(t) = \delta^{18} O_{DCP}^{EQ} + \left( \delta^{18} O_{DCP}^{t=0} - \delta^{18} O_{DCP}^{EQ} \right) \cdot \exp(-t/\tau)$$
(6)

where  $\delta^{18} O_{DCP}^{f=0}$  and  $\delta^{18} O_{DCP}^{EQ}$  are  $\delta^{18} O$  of DCP at the initial and equilibrium condition. This first-order decay function draws a simple unidirectional and asymptotic trajectory towards the full  $\delta^{18} O$  equilibrium. Note that it is also possible to express Eq. (6) in terms of oxygen isotope fractionation between DCP and  $H_2O$ , when  $\delta^{18}O$  of  $H_2O$  is known (see UZ12).

Tripati et al. (2015) reported a measurable  $\Delta_{47}$  offset of 0.063% between HCO<sub>3</sub><sup>-</sup> and CO<sub>3</sub><sup>2-</sup> (0.713\% and 0.650\%, respectively) at 25 °C, which can be applied to a similar mass balance to model the pH-induced shift in the equilibrium  $\Delta_{47}$  signature of DCP (Fig. 1d). For their study, Tripati et al. (2015) used BaCO<sub>3</sub> samples quantitatively precipitated from NaHCO<sub>3</sub> solutions, whose δ<sup>18</sup>O of DCP was in full equilibrium with H<sub>2</sub>O (Uchikawa and Zeebe, 2013). But, at that time, it was still untested whether  $\Delta_{47}$  equilibrium in DCP can be achieved on a similar timescale as δ<sup>18</sup>O equilibrium. Staudigel and Swart (2018) (denoted as SS18 hereafter) represents the first study that characterized and compared the kinetics of  $\delta^{18}$ O and  $\Delta_{47}$  equilibration in DCP. Their data show that DCP comes to equilibrium on a similar timescale for both  $\delta^{18}O$  and  $\Delta_{47}$ . This is consistent with Affek (2013) and Clog et al. (2015), who studied the same subject, but between CO<sub>2(gas)</sub> and H<sub>2</sub>O. SS18 also found a distinctive non-first-order kinetics in the attainment of  $\Delta_{47}$  equilibrium in DCP, such that the system initially heads to even stronger disequilibrium before a subsequent

Fig. 1. (a) DIC speciation as a function of pH for freshwater at [DIC] = 15 mM and  $T = 25 \,^{\circ}\text{C}$ , using the algorithm of Zeebe and Wolf-Gladrow (2001). DIC is almost exclusively contributed by HCO<sub>3</sub><sup>-</sup> (solid line) and CO<sub>3</sub><sup>2-</sup> (dashed line) at the pH range shown here. (b) The overall equilibrium oxygen isotope fractionation between DCP (Dissolved Carbonate Pool =  $[HCO_3^-] + [CO_3^{2-}]$ ) and H<sub>2</sub>O as a function of pH, adapted from Zeebe (2007). The fractionation is expressed as  $\varepsilon$  in % (where  $\varepsilon = (\alpha - 1) \times 10^3$ ). The projection shown here is based on  $^{18}\alpha^{EQ}_{CO2(aq)-H2O}$  as a function of T by Beck et al. (2005) and  $^{18}\alpha^{EQ}_{HCO3-H2O}$  and  $^{18}\alpha^{EQ}_{CO3-H2O}$  established at 25 °C by Uchikawa and Zeebe (2013). (c) pH-dependence of  $\delta^{18}$ O equilibration kinetics based on UZ12 (also see Usdowski et al., 1991). The equilibration rate constant  $\tau^{-1}$  (solid black curve) decreases with pH due to a decline in  $[CO_{2(aq)}]$ , invoking longer  $\delta^{18}$ O equilibration in DCP as shown by " $T_{EQ}$ " (dashed red curve). (d) Expected equilibrium  $\Delta_{47}$  of DCP as a function of pH, based on mass-balance calculations using the end-member  $\Delta_{47}$  of  $0.713 \pm 0.001\%$  and  $0.650 \pm 0.006\%$  for HCO $_3^-$  and CO $_3^{2-}$  by Tripati et al. (2015). The gray shading represents the propagated uncertainties in the end-member  $\Delta_{47}$  values. The vertical bandings in blue and orange color indicate the experimental pH<sub>NBS</sub> of UZ12  $(\sim 8.9)$  and SS18 (9.2-9.4), respectively.

turn-around and eventual continuous approach towards equilibrium. This creates a characteristic "dip" in the  $\Delta_{47}$  equilibration trajectory (see Fig. S1 in the Supplementary Materials). More recently, however, Weise and Kluge (2020) reported contrasting experimental data showing no clear non-first-order pattern.

This prompted us to launch an independent investigation on  $\Delta_{47}$  equilibration kinetics, specifically by analyzing  $\Delta_{47}$  of the BaCO<sub>3</sub> samples by UZ12, which were quantitatively precipitated from NaHCO<sub>3</sub> solutions at various times over the course of  $\delta^{18}$ O equilibration. UZ12 also examined δ<sup>18</sup>O equilibration kinetics in the presence of carbonic anhydrase (CA), an enzyme highly effective in catalyzing CO<sub>2</sub> hydration (Eq. (3)). Since CO<sub>2</sub> hydration is a major bottleneck for oxygen isotope exchange between DCP and H<sub>2</sub>O and since various marine calcareous organisms possess this enzyme (Tambutté et al., 2007; Moya et al., 2008; Bertucci et al., 2011; de Goeyse et al., 2021; Zhang et al., 2021), potential implications of CA on both isotopic paleothermometers have drawn significant interests (UZ12; Saenger et al., 2012; Watkins et al., 2013; 2014; Tripati et al., 2015; Kelson et al., 2017; Chen et al., 2018; Thaler et al., 2020). For this reason, we additionally analyzed the BaCO<sub>3</sub> samples precipitated from the NaHCO<sub>3</sub> solutions with CA in order to characterize and compare  $\Delta_{47}$  equilibration kinetics under normal (uncatalyzed, without CA) and enzymatically catalyzed conditions.

#### 2. MATERIALS AND METHODS

# 2.1. Sample descriptions

The BaCO<sub>3</sub> samples analyzed here were quantitatively precipitated from NaHCO3 solutions at various times over the course of  $\delta^{18}$ O equilibration at 25 °C and pH<sub>NBS</sub> of ~8.9 by UZ12. Quantitative precipitation refers to a quasiinstantaneous and complete transformation of DCP into solid carbonate minerals, so that the isotopic state of DCP at the time of precipitation can be preserved (UZ12; Beck et al., 2005). The NaHCO<sub>3</sub> solutions were prepared to 15 mM by dissolving isotopically homogeneous NaHCO<sub>3</sub> powder into N<sub>2</sub>-bubbled (i.e., CO<sub>2(aq)</sub>-free) deionized H<sub>2</sub>O at 25 °C. A fixed volume of 0.5 M NaOH solution prepared from the same H<sub>2</sub>O was also added to adjust solution pH. For the experiments with CA enzyme, the solutions were supplemented with bovine CA solution (see UZ12 for details). The NaHCO<sub>3</sub> solutions were directly prepared into individual serum bottles with negligible headspace. The bottles were immediately transferred into 25 °C water bath for isotopic equilibration. Then, they were used for BaCO<sub>3</sub> precipitation in a time-series fashion over the course of equilibration by reacting with excess BaCl<sub>2</sub>•2H<sub>2</sub>O powder and 2.5 M NaOH solution. From individual bottles of NaHCO3 solution used at discrete times, two replicate BaCO<sub>3</sub> samples were produced within a time separation of only 1 to 2 minutes.

We selected sample subsets from TS2, TS2-mnCA, TS2-2CA and TS2-3CA series (see Table 2 in UZ12). The

TS2 series represents a normal condition, in which no CA enzyme was added to the NaHCO3 solutions. The others (TS2-mnCA, TS2-2CA and TS2-3CA) represent enzymatically catalyzed conditions, to which bovine CA was added to concentrations of 3.7, 9.3 and 19 nM, respectively. The BaCO3 yields for all sample subsets ranged from 94.3 to 102.2% of the theoretical yield and their  $\delta^{13}$ C values agreed well with  $\delta^{13}$ C of the NaHCO3 used in their experiments (UZ12). This stoichiometric and isotopic evidence validate the quantitative nature of the BaCO3 samples.

We were able to re-analyze aliquots of the experimental NaHCO<sub>3</sub> for stable isotopes, but archives of the experimental H<sub>2</sub>O were no longer available. The original  $\delta^{18}O_{H2O}$  data reported in UZ12 is used when necessary.

#### 2.2. Stable isotope analyses and definitions

The BaCO<sub>3</sub> samples and aliquots of the experimental NaHCO<sub>3</sub> were analyzed at the California Institute of Technology (Caltech) for  $\delta^{13}$ C,  $\delta^{18}$ O and  $\Delta_{47}$  on a Thermo MAT253 dual-inlet isotope ratio mass spectrometer, as detailed elsewhere (Bonifacie et al., 2017; Lloyd et al., 2019; Chen et al., 2019). About 17 mg of the BaCO<sub>3</sub> samples or 10 mg of the NaHCO<sub>3</sub> was digested with 104% phosphoric acid at 90 °C in a common acid bath. Five replicates of NaHCO<sub>3</sub> were analyzed, while each BaCO<sub>3</sub> sample was analyzed either once or twice. The resultant CO<sub>2(gas)</sub> was cryogenically purified and passed through a Porapaq Q (50/80 mesh) GC column held at -20 °C to eliminate organic contaminants. The purified sample CO<sub>2(gas)</sub> was analyzed for masses 44 to 49 against a reference CO<sub>2(gas)</sub> externally calibrated with the NBS-19 reference material. The TS2, TS2-mnCA and TS2-2CA samples and the NaHCO<sub>3</sub> aliquots were analyzed from October to November 2018, and the TS2-3CA samples were analyzed in November 2019.

Stable C and O isotope data are given by the conventional  $\delta$  notation in permil (‰):

$$\delta = \left(\frac{R_{\text{Sample}}}{R_{\text{Standard}}} - 1\right) \cdot 10^3 \tag{7}$$

where R is the isotope ratio  $^{13}\text{C}/^{12}\text{C}$  ( $^{13}R$ ) for  $\delta^{13}\text{C}$  or  $^{18}\text{O}/^{16}\text{O}$  ( $^{18}R$ ) for  $\delta^{18}\text{O}$ . While  $\delta^{13}\text{C}$  and  $\delta^{18}\text{O}$  of the carbonate phases (BaCO<sub>3</sub> and NaHCO<sub>3</sub>) are reported on the VPDB scale,  $\delta^{18}\text{O}$  of H<sub>2</sub>O (UZ12) are on the VSMOW scale. We followed Coplen et al. (1983) for rescaling VPDB to VSMOW for  $\delta^{18}\text{O}$  of the carbonates:

$$\delta^{18}O_{VSMOW} = 1.03091 \cdot \delta^{18}O_{VPDB} + 30.91\%$$
 (8)

The apparent oxygen isotope fractionations between the carbonates and  $H_2\mathrm{O}$  were then calculated in permil as:

$${}^{18}\varepsilon_{\text{Carbonate-H2O}} = ({}^{18}\alpha_{\text{Carbonate-H2O}} - 1) \cdot 10^3 \tag{9}$$

vhere

$$^{18}\alpha_{\text{Carbonate-H2O}} = (\delta^{18}O_{\text{Carbonate}} + 10^3) / (\delta^{18}O_{\text{H2O}} + 10^3)$$
(10)

For clumped isotopes, the quantity  $\Delta_{47}$  is defined as:

$$\Delta_{47} = \left[ \left( \frac{^{47}R_{\text{Measured}}}{^{47}R^*} - 1 \right) - \left( \frac{^{46}R_{\text{Measured}}}{^{46}R^*} - 1 \right) - \left( \frac{^{45}R_{\text{Measured}}}{^{45}R^*} - 1 \right) \right] \cdot 10^3$$
(11)

where  ${}^{47}R$ ,  ${}^{46}R$  and  ${}^{45}R$  are the abundance ratio of rare isotopologues to the unsubstituted mass 44 isotopologue (*i.e.*,  ${}^{12}C^{16}O^{16}O$ ). The  ${}^{i}R^*$  are the corresponding ratios for stochastic isotope distribution, which depend on the bulk  $\delta^{13}C$  and  $\delta^{18}O$  (Eiler, 2011):

$$\Delta_{47} = \left[ \frac{{}^{47}R}{2^{-13}R^{-18}R + 2^{-17}R^{-18}R + {}^{-13}R({}^{-17}R)^2} - \frac{{}^{46}R}{2^{-18}R + 2^{-13}R^{-17}R + ({}^{-17}R)^2} - \frac{{}^{45}R}{{}^{-13}R + 2^{-17}R} + 1 \right] \cdot 10^3$$
(12)

Following Brand et al. (2010),  $\Delta_{47}$  values were calculated using  $^{13}R$  ratio for VPDB and  $^{17}R$  ( $^{17}O/^{16}O$ ) and  $^{18}R$  ratios for VSMOW to minimize inter- and intra-laboratory discrepancies for  $\Delta_{47}$  determinations (Schauer et al., 2016; Daëron et al., 2016). The final  $\Delta_{47}$  values and measurement uncertainties were calculated in the absolute reference frame (ARF) of Dennis et al. (2011), following Daëron et al. (2016).

Both the BaCO<sub>3</sub> samples and NaHCO<sub>3</sub> aliquots were treated as calcite. In other words,  $\delta^{18}O$  and  $\Delta_{47}$  values reported here were not corrected with BaCO<sub>3</sub>-specific or NaHCO<sub>3</sub>-specific acid fractionation factors (AFF). To the best of our knowledge, the NaHCO<sub>3</sub>-specific AFF for both  $\delta^{18}$ O and  $\Delta_{47}$  are unknown. Though some studies attempted to establish the BaCO<sub>3</sub>-specific AFF for  $\delta^{18}$ O and its dependence to the mineral-acid reaction temperature, they appear somewhat questionable at this stage (see Uchikawa and Zeebe (2013) for further discussions). Tripati et al. (2015) compared the AFFs for  $\Delta_{47}$  measurements on calcite and BaCO<sub>3</sub> and found their difference to be 0.025%, which is comparable to an estimated 0.015% difference by Guo et al. (2009) based on transition state theory. But, to be consistent with SS18, we did not take this into account for our  $\Delta_{47}$  data.

Typical measurement uncertainty was 0.005% for  $\delta^{13}$ C and 0.008% for  $\delta^{18}$ O (1SE, standard error of individual samples). For clumped isotopes, the standard error (shot noise limited) of individual  $\Delta_{47}$  measurements was on average 0.011%. After correction to the absolute reference frame with equilibrated gases at 25 and 1000 °C (Dennis et al., 2011), the average 1SE for individual samples was 0.014%. Two in-house carbonate standards were routinely analyzed to check the long-term reproducibility of the measurements. Across three different analytical sessions, we obtained  $\Delta_{47}$  values of 0.401  $\pm$  0.006% (1SE, n=19) for Carrara Marble and  $0.664 \pm 0.005\%$  (1SE, n = 18) for TV04 travertine, both within errors of their long-term average values (0.405  $\pm$  0.020% for Carrara Marble and 0.65  $5 \pm 0.020\%$  for TV04). However, there were systematic drifts in  $\Delta_{47}$  values for the carbonate standards in different analytical sessions. We hence applied session-specific stretching corrections to our samples based on the values measured on the carbonate standards and their long-term average values. The external reproducibility ( $\Delta_{47}$  offset across analytical sessions) of replicate measurements on our inorganic BaCO<sub>3</sub> samples was 0.020‰ on average.

#### 2.3. Numerical modeling

Our experimental data are interpreted with two numerical models. The first is an adapted version of the model by SS18, which exclusively performs non-linear regression on a set of time-series isotope data to derive the rate constant for changes in singly- and doubly-substituted species in DCP ( $[^{12}C^{18}O^{16}O^{16}O]$  and  $[^{13}C^{18}O^{16}O^{16}O]$ , respectively). However, this model is not designed to simulate the progress of isotopic equilibration under various conditions with a unique physicochemical state (e.g., pH and temperature). This led us to come up with an entirely independent model by extending the framework of Chen et al. (2018) with some modifications adopted from Christensen et al. (2021). This model is referred to as the ExClump38 model (Model for Exchange and Clumping of <sup>13</sup>C and <sup>18</sup>O in DCP). Unlike the SS18 model, the ExClump38 model enables simulations of chemical and isotopic ( $\delta^{13}$ C,  $\delta^{18}$ O and  $\Delta_{47}$ ) evolution in DCP from a set of equilibrium and kinetic constants and isotope fractionation factors compiled from the literature. We used this model to identify key fractionation factors controlling the  $\Delta_{47}$  equilibration trajectory (Section 4.4.1) and to simulate the timescales and trajectories of isotopic equilibration for various hypothetical scenarios (Section 4.4.3). To further describe the two models, we follow the notations used by UZ12 (2) and 3 for  $^{12}$ C and  $^{13}$ C, 6 and 8 for  $^{16}$ O and  $^{18}$ O in/from CO<sub>2(aq)</sub> and H<sub>2</sub>O, and 6' and 8' for  $^{16}$ O and  $^{18}$ O in association with OH<sup>-</sup>).

## 2.3.1. **SS18** model

The basic concept of the SS18 model is as follows. Practically,  $\delta^{18}O$  is a measure of mass 46 signal over 44 in  $CO_2$  (gas) from acid digestion of carbonate samples, which in turn depends on the abundance of  $^{18}O$ -substituted carbonate species ( $^{12}C^{18}O^{16}O^{16}O$ , or 2866 for short) over unsubstituted species (2666) in the samples. The time-course of  $\delta^{18}O$  equilibration therefore reflects the evolution of 2866 in DCP, for instance, as unsubstituted  $CO_{2(aq)}$  (266(aq)) gains  $^{18}O$  from  $H_28$  or  $8'H^-$  (via Eq. (3) and/or Eq. (4)):

$$[2866](t) = [2866]^{EQ} + ([2866]^{t=0} - [2866]^{EQ}) \cdot \exp(-k_{46} \cdot t)$$
(13)

Though expressed slightly differently, this equation is no different from Eq. (6), and the rate constant  $k_{46}$  here corresponds to  $1/\tau$  in Eq. (6) (also in Eq. (5)). Thus, there should be a reasonable agreement between the experimentally-derived  $k_{46}$  and theoretical  $\tau^{-1}$  for successful time-series quantitative BaCO<sub>3</sub> precipitation experiments under normal uncatalyzed conditions (see UZ12). On the other hand,  $\Delta_{47}$  is a measure of the abundance of  $^{13}\text{C}_{-}^{18}\text{O}$  bonds in the acid liberated CO<sub>2(gas)</sub> (*i.e.*, mass 47 over 44), which is contributed by  $386_{(gas)}$  originating mainly from 3866 in the carbonate samples (Ghosh et al., 2006). The temporal change

in [3866] in DCP (as  $366_{(aq)}$  reacts with  $H_28$  or  $8'H^-$ ) should follow a similar rate law, but with a different rate constant (Clog et al., 2015; SS18):

$$[3866](t) = [3866]^{EQ} + ([3866]^{t=0} - [3866]^{EQ}) \cdot \exp(-k_{47} \cdot t)$$
 (14)

SS18 used the expression  $\delta^{18}O_{C13}$  for [3866], which was defined as  $\delta^{18}O$  of oxygen bound to  $^{13}C.$  For conventional  $\delta^{13}$ C and  $\delta^{18}$ O, a kinetic isotope effect (KIE) is said to occur if there is a difference in the rate of a given reaction involving the heavy and light isotopes. Then, if  $k_{46}$  and  $k_{47}$  differ, this can be likewise considered as a KIE for clumped isotope systems (SS18). Following SS18, this is referred to as <sup>13-18</sup>KIE:

$$^{13-18}KIE = k_{47}/k_{46} \tag{15}$$

The SS18 model calculates the rate constants  $k_{46}$  and  $k_{47}$  (hence  $^{13-18}$ KIE) as well as the initial and equilibrium condition for  $\delta^{18}$ O and  $\Delta_{47}$  of DCP by MATLAB's nonlinear regression. The core of the model is two MATLAB functions "unclump" and "clump". While the former iteratively estimates  $\delta^{18}O_{C13}$  from  $\delta^{13}C$ ,  $\delta^{18}O$  and  $\Delta_{47}$  measured on samples, the latter performs reverse  $\Delta_{47}$  modeling from the estimated  $\delta^{18}O_{C13}$  along with  $\delta^{13}C$  and  $\delta^{18}O$  data (see SS18 for details). We found that their model in its original form did not provide an ideal fit to our data, especially in terms of the magnitude of the dip in the  $\Delta_{47}$  equilibration trajectory. It is likely that the regression is skewed more towards the tail end of the time-series data in our case, as there are considerably more data-points near and after equilibrium. The other issue is the noise in our  $\Delta_{47}$  data, which is larger than in the SS18 data (see below). These factors likely caused relatively poor model-data agreement for our datasets. To overcome this issue, we implemented some simple optimizations to the SS18 model.

We first obtained the rate constant  $k_{46}$  by fitting the exponential function (Eq. (13)) to our  $\delta^{18}O$  data via nonlinear regression (as is the case in SS18). But, unlike SS18, we optimized the fit to accept a specific value for  $\delta^{18}O^{t=0}$  and  $\delta^{18}O^{EQ}$  of DCP. Similarly, the values for the initial and equilibrium condition ( $\delta^{18}O_{C13}^{t=0}$  and  $\delta^{18}O_{C13}^{EQ}$ ) were manually set to fit Eq. (14) to the  $\delta^{18}O_{C13}$  time-series derived from the unclump function. Then, based on the relationship given by Eq. (15), the rate constant  $k_{47}$  was set by  $k_{46}$  obtained from the first step and a manually assigned  $^{13-18}$ KIE, for which a range of values were tested. Finally,  $\delta^{18}O$  and  $\delta^{18}O_{C13}$  as a function of time modeled by the resultant exponential functions (Eqs. (13) and (14)) were processed by the clump function to compute  $\Delta_{47}$  as a function of time. The first  $\delta^{18}O$  and  $\delta^{18}O_{C13}$  point in each timeseries was used as the input for  $\delta^{18}O^{t=0}$  and  $\delta^{18}O^{t=0}_{C13}$ . For  $\delta^{18}O^{EQ},$  we used the average of the  $\delta^{18}O$  data constituting the well-defined equilibrium plateau (e.g., Fig. 3b). The average of the corresponding  $\delta^{18}O_{C13}$  computed for those post-equilibrium data-points by the unclump function was adopted as the initial guess for  $\delta^{18}O_{CI3}^{EQ}$ . However, uncertainty and noise in our isotope data (especially in  $\Delta_{47}$ ) heavily influenced  $\delta^{18}O_{C13}^{EQ}$  to be applied for the fitting and the final  $\Delta_{47}$  model output (Fig. S2). To take this into account,

we allowed a freedom for  $\delta^{18}O_{C13}^{EQ}$  to vary within  $\pm~1\sigma$  S.D. associated with the averaging. In short, we searched for a combination of  $^{13\text{-}18}\text{KIE}$  and  $\delta^{18}\text{O}^{\text{EQ}}_{\text{Cl}3}$  that gives the optimum model-data agreement in  $\Delta_{47}$ , as those parameters were the key factors that shape the overall curvature of the  $\Delta_{47}$  equilibration trajectory (Fig. S3). The goodness of the model fit to the experimental data was evaluated by median symmetric accuracy (MdSA) by Morley et al.

$$MdSA = \left[ exp \left\{ Md_{i=1}^{n} (|log_{e}Q_{i}|) \right\} - 1 \right] \cdot 100(\%)$$
 (16)

where  $Md_{i-1}^n$  is the median of the numbers  $|log_e Q_i|$  for i=1,  $2, \ldots, n$  and Q is the ratio of the model predicted value to the observed data (the accuracy ratio). Note that MdSA penalizes model over- and under-forecasts equally, which is not necessarily the case for other more common measures for model performance such as the mean absolute percent error (for other practical advantages for MdSA, see Morley et al., 2018). We tested our optimized approach using the SS18 25 °C dataset, and the inputs for optimum model-data agreement were <sup>13-18</sup>KIE = 0.980 and  $\delta^{18}O_{C13}^{EQ} = -2.24\%$  (Table 1; Fig. S4). This <sup>13-18</sup>KIE value agrees well with the original value reported in SS18  $(0.981 \pm 0.007)$ , which provides confidence in our optimized approach.

## 2.3.2. ExClump38 model

Chen et al. (2018) developed a model to simulate the chemical,  $\delta^{13}$ C and  $\delta^{18}$ O evolution in DCP of the coral extracellular calcifying fluid during active calcification. After omitting some unnecessary processes (diffusion, mixing, CaCO<sub>3</sub> precipitation, etc.) and tracers (Ca<sup>2+</sup> and alkalinity) for our applications here, we extended the model to additionally simulate the evolution of doubly-substituted isotopologues (i.e.,  $\Delta_{47}$ ) with some adaptations from Christensen et al. (2021). We name this version as the ExClump38 model.

The ExClump38 model traces the chemical and isotopic evolution in DCP, which depends on CO2 hydration and unsubstituted, singlyhydroxylation involving doubly-substituted species:

$$266 + H_2 6 \underset{k_{-1}}{\overset{k_{+1}}{\rightleftharpoons}} H2666^- + H^+ \tag{17}$$

$$266 + 6'H^{-} \underset{k_{-4}}{\overset{k_{+4}}{\rightleftharpoons}} H2666^{-} \tag{18}$$

$$366 + H_2 6 \stackrel{^{13}k_{+1}}{\underset{^{13}k_{-1}}{\rightleftharpoons}} H3666^- + H^+ \tag{19}$$

$$366 + 6' \text{H}^{-} \stackrel{^{13}k_{+4}}{\underset{^{13}k_{-4}}{\leftrightharpoons}} \text{H}3666'^{-} \tag{20}$$

$$266 + H_2 8 \underset{\frac{1}{3}^{a_{-1}}}{\stackrel{a_{+1}}{\rightleftharpoons}} H2668^- + H^+ \tag{21}$$

$$286 + \text{H}_{2}6 \underset{\frac{2}{3}b_{-1}}{\rightleftharpoons} \text{H}_{2}866^{-} + \text{H}^{+}$$

$$266 + 8'\text{H}^{-} \underset{\frac{1}{3}a_{-4}}{\rightleftharpoons} \text{H}_{2}668'^{-}$$
(23)

$$266 + 8'H \stackrel{\stackrel{a_{,44}}{\rightleftharpoons}}{\underset{\frac{1}{3}a_{-4}}{\rightleftharpoons}} H2668'^{-}$$
 (23)

Table 1 Comparison of the rate constants for Eq. (13) and Eq. (14) (k46 and k47) and 13-18 KIE derived from our experimental series using the optimized SS18 model (see Section 2.3.1). Also compared is the  $\delta^{18}$ O equilibration rate constant  $\tau^{-1}$  calculated at respective experimental pH (Usdowski et al., 1991; Zeebe and Wolf-Gladrow, 2001; UZ12). For successful time-series quantitative carbonate (in this case, BaCO<sub>3</sub>) precipitation experiments, there should be a good agreement between  $\tau^{-1}$  and experimentally derived  $k_{46}$ .

	Uncatalyzed conditions		CA-Catalyzed conditions			
	SS18 25 °C Data Original	SS18 25 °C Data Re-evaluated	TS2	TS2-mnCA	TS2-2CA	TS2-3CA
$k_{46}  (\mathrm{min}^{-1})$ $\delta^{18} \mathrm{O}^{EQ}  (\%e)$ $k_{47}  (\mathrm{min}^{-1})$ $\delta^{18} \mathrm{O}^{EQ}_{\mathrm{C13}} (\%e)$ $^{13-18} \mathrm{KIE}$ MdSA $(\%)^{\dagger}$	$ \begin{array}{c} 10.03 \times 10^{-3} \\ -2.85 \\ 9.84 \times 10^{-3} \\ -0.981 \pm 0.007 \end{array} $	$   \begin{array}{r}     10.03 \times 10^{-3} \\     -2.90 \\     9.83 \times 10^{-3} \\     -2.24 \\     0.980 \\     1.55   \end{array} $	$4.99 \times 10^{-3}$ $-3.75$ $4.88 \times 10^{-3}$ $-3.02$ $0.978$ $2.05$	$   \begin{array}{r}     10.86 \times 10^{-3} \\     -3.86 \\     10.60 \times 10^{-3} \\     -3.14 \\     0.976 \\     1.37   \end{array} $	28.75×10 <sup>-3</sup> -3.99 28.08×10 <sup>-3</sup> -3.26 0.977 0.88	$68.15 \times 10^{-3}$ $-3.90$ $66.43 \times 10^{-3}$ $-3.21$ $0.975$ $2.31$
Theoretical $\tau^{-1}$ from UZ12 model (min <sup>-1</sup> )	$(3.83 \text{ to } 4.24) \times 10^{-3}$	$(3.83 \text{ to } 4.24) \times 10^{-3}$	$4.75 \times 10^{-3}$	_	_	_

<sup>†:</sup> Goodness of model-data agreement for the  $\Delta_{47}$  equilibration trajectory measured as Median Symmetric Accuracy (Eq. (16)).

$$286 + 6'H^{-} \underset{\stackrel{b_{+4}}{\rightleftharpoons}}{\rightleftharpoons} H2866'^{-}$$

$$366 + H_{2}8 \underset{\stackrel{p_{+1}}{\rightleftharpoons}}{\rightleftharpoons} H3866^{-} + H^{+}$$

$$386 + H_{2}6 \underset{\stackrel{s_{+1}}{\rightleftharpoons}}{\rightleftharpoons} H3866^{-} + H^{+}$$

$$(25)$$

$$366 + H_2 8 \underset{\frac{1}{2}p_{-1}}{\overset{p_{+1}}{\rightleftharpoons}} H3866^- + H^+ \tag{25}$$

$$386 + H_26 \stackrel{s_{+1}}{\rightleftharpoons} H3866^- + H^+ \tag{26}$$

$$366 + 8'H^{-} \underset{\$^{p-4}}{\overset{p_{+4}}{\rightleftharpoons}} H38'66^{-} \tag{27}$$

$$386 + 6'H^{-} \underset{\frac{2}{5}^{5} - 4}{\overset{s_{+4}}{\rightleftharpoons}} H3866'^{-}$$
 (28)

The subscripts  $\pm 1$  and  $\pm 4$  for the rate constants signify CO<sub>2</sub> hydration/dehydration and hydroxylation/dehydroxy lation. The rate constants for <sup>13</sup>C exchange are labeled as <sup>13</sup>k's (Eq. (19) and Eq. (20)). After Chen et al. (2018), the rate constants for <sup>18</sup>O-substituted species are given by a's or b's. While a's are for the reactions where  $^{18}$ O originates from or ends up in H<sub>2</sub>O or OH<sup>-</sup>, b's are for the reactions where  $^{18}O$  comes from or goes to  $CO_{2(aq)}$  (Eq. (22) and Eq. (24)). We follow Guo (2020) for the notation of the rate constants for Eq. (25) to Eq. (28), where p's are for the primary reactions involving new formation or break-up of  $^{13}\text{C-}^{18}\text{O}$  bonds during the conversion between  $\text{CO}_{2(aq)}$  and  $HCO_3^-$  (Eq. (25) and Eq. (27)) and s's are for the secondary reactions with no  $^{13}C_2^{-18}O$  formations or break-ups (Eq. (26) and Eq. (28)). The 2/3 and 1/3 factors applied to the reverse rate constants (Eq. (21) to Eq. (28)) are adopted from Christensen et al. (2021) and signify the fact that, of 1 unit of HCO<sub>3</sub> undergoing dehydration or dehydroxylation, 2/3 of the oxygen atoms go to CO<sub>2</sub> and 1/3 go to H<sub>2</sub>O or OH<sup>-</sup>. Note also that we assume Eq. (17) and Eq. (18) for the unsubstituted species to be the same as Eq. (3) and Eq. (4). Then, following the scheme of Mills and Urey (1940) (also see UZ12; Chen et al., 2018; Christensen et al., 2021), the exchange reactions above lead to a set of eight differential equations describing the changes in concentration and isotopic state of CO<sub>2(aq)</sub> and DCP over time, which are numerically solved by MATLAB's ode15s solver with input variables (e.g.,

temperature, pH, initial  $\delta^{13}$ C,  $\delta^{18}$ O and  $\Delta_{47}$  of DCP, etc.). As given in the full description of the ExClump38 model in the Supplementary Materials, the differential equations become a function of equilibrium constants  $(K_1, K_2)$  and  $K_{\rm W}$ ), kinetic rate constants for CO<sub>2</sub> hydration and hydroxylation  $(k_{+1} \text{ and } k_{+4}, \text{ see Eq. (3)} \text{ and Eq. (4)})$ , equilibrium C and O isotope fractionations of the dissolved carbonate system ( $^{13}\alpha^{EQ}$ 's and  $^{18}\alpha^{EQ}$ 's), kinetic C and O isotope fractionation factors ( $^{13}\alpha^{KIF}$ 's and  $^{18}\alpha^{KIF}$ 's) and intrinsic KIE for clumped isotopes for CO<sub>2</sub> hydration and hydroxylation (<sup>47</sup>KIE's: see Section 4.4.1). These constants and fractionation factors were compiled from the literature (Harned and Scholes, 1941; Harned and Davis, 1943; Pinsent et al., 1956; Harned and Owen, 1958; Zhang et al., 1995; Beck et al., 2005; Uchikawa and Zeebe, 2013; Tripati et al., 2015; Guo, 2020; Zeebe, 2020; Yumol et al., 2020; Christensen et al., 2021). Finally, the effect of CA enzyme was implemented as the enhancement factor for the rate constants associated with CO<sub>2</sub> hydration. The formulation of the enhancement factor as a function of enzyme concentrations directly follows the Michaelis-Menten kinetic model by UZ12:

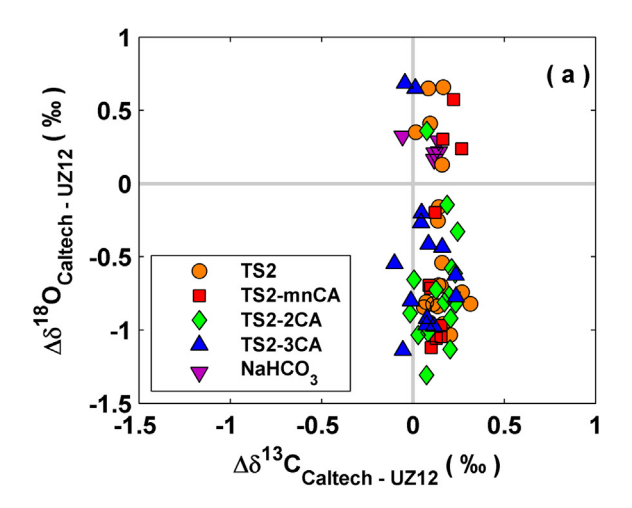
Enhacement Factor = 
$$\frac{k_{+1} + \frac{k_{Cat}}{k_M} \cdot [CA]}{k_{+1}}$$
 (29)

where  $K_M$  and  $k_{\text{cat}}$  is the Michaelis-Menten constant and catalytic rate constant, respectively (see Section 5.3 in UZ12 for more details). The rate enhancement factor was equally applied to  $k_{\pm 1}$ ,  $^{13}k_{\pm 1}$ ,  $a_{\pm 1}$ ,  $b_{\pm 1}$ ,  $p_{\pm 1}$  and  $s_{\pm 1}$ (Eq. (17), Eq. (19), Eq. (21), Eq. (22), Eq. (25) and Eq. (26)) by assuming no additional isotope effect from CA (e.g., Chen et al., 2018). The codes for the ExClump38 model are accessible via the EarthChem Library data repository system (https://doi.org/10.26022/IEDA/112078).

## 3. RESULTS

Our new isotope data generated at Caltech are given in Table S1 (Supplementary Materials). Our new data in Table S1 are also compared to the original data by UZ12, which were measured at the University of California Santa Cruz (UCSC) for the BaCO<sub>3</sub> samples and at the University of California Davis for aliquots of the experimental NaHCO<sub>3</sub>. Relative to the original UZ12 data,  $\delta^{13}C_{BaCO3}$  values newly measured at Caltech were consistently higher by ~0.2%. In contrast, the differences in  $\delta^{18}O_{BaCO3}$  values were more variable and ranged roughly from -1.2% to +0.6% between our values and UZ12 (Fig. 2). But these differences are small compared to the overall range of  $\delta^{18}$ -  $O_{BaCO3}$  values explored here (see Section 4.1).

The average  $\delta^{13}$ C and  $\delta^{18}$ O of the experimental NaHCO<sub>3</sub> was  $-2.78 \pm 0.08\%$  and  $-15.63 \pm 0.64\%$  (VPDB,  $\pm 1\sigma$  SD., n=5). For the BaCO<sub>3</sub> samples,  $\delta^{13}$ C ranged narrowly from -3.25% to -2.98%. In all experimental series,  $\delta^{13}$ C values of BaCO<sub>3</sub> were fairly constant irrespective of the elapsed equilibration time and closely agreed with  $\delta^{13}$ C of the NaHCO<sub>3</sub> (Fig. 3a and Fig. 4adg). This validates the quantitative nature of our BaCO<sub>3</sub> sam-



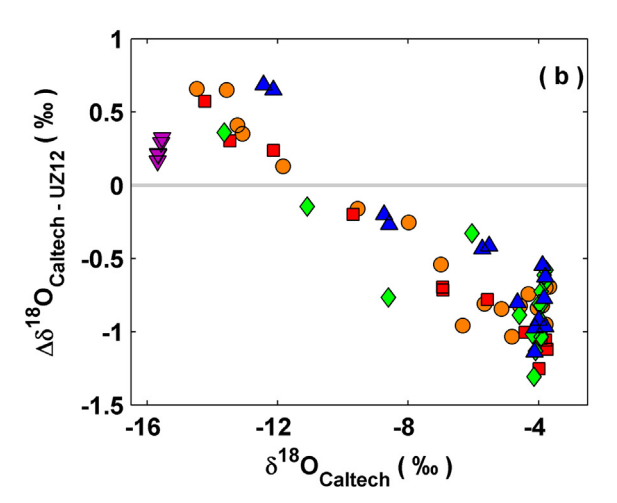


Fig. 2. (a) Comparison of our newly measured  $\delta^{13}C_{VPDB}$  and  $\delta^{18}O_{VPDB}$  values of the BaCO<sub>3</sub> samples and experimental NaHCO<sub>3</sub> to the original data reported in UZ12. (b) Comparison of the  $\delta^{18}O_{VPDB}$  offsets to the actual sample  $\delta^{18}O_{VPDB}$  values determined at Caltech. Notice that the data from all of the experimental series show the same trend.

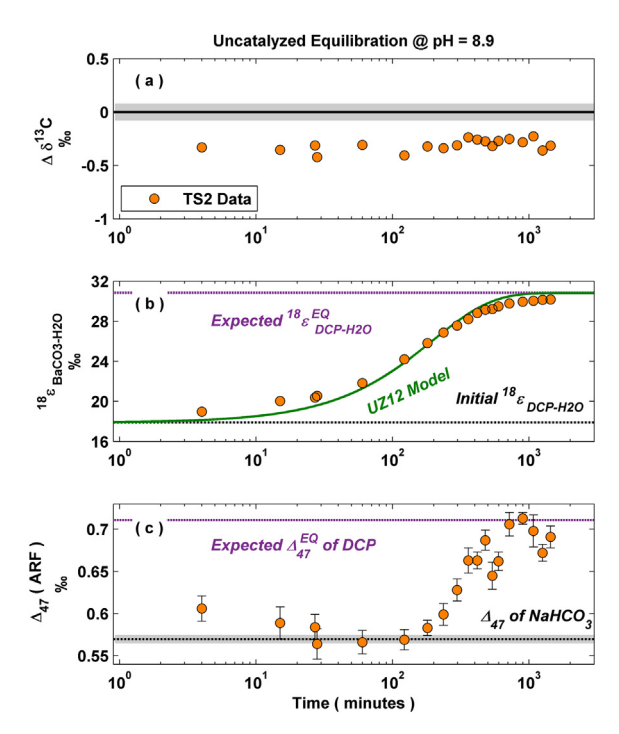


Fig. 3. Summary of our new isotope data from TS2 experimental series, in the absence of enzyme carbonic anhydrase. (a) Difference in  $\delta^{13}C_{VPDB}$  between the BaCO<sub>3</sub> samples and the experimental NaHCO<sub>3</sub>. The gray horizontal banding represents  $\pm 1\sigma$  SD of δ<sup>13</sup>C<sub>NaHCO3</sub> measured on 5 aliquots. (b) Temporal change in oxygen isotope fractionation between DCP and H<sub>2</sub>O reflected by the TS2 BaCO<sub>3</sub> samples. The initial condition (dash-dotted black line) is calculated from δ<sup>18</sup>O of the experimental NaHCO<sub>3</sub> and H<sub>2</sub>O, whereas the expected equilibrium condition (dashed purple line) is from Fig. 1b. Also overlaid in the panel is the  $\delta^{18}$ O equilibration trajectory based on the UZ12 model (green curve). (c) Temporal change in  $\Delta_{47}$  of DCP reflected by the TS2 BaCO<sub>3</sub> samples. Also compared in the panel is  $\Delta_{47}$  of the experimental NaHCO<sub>3</sub> (dash-dotted black line) and expected  $\Delta_{47}$  of DCP at equilibrium (dashed purple line), which is from Fig. 1d. The error bars for the isotope data are  $\pm$  1SE.

ples, as previously discussed in UZ12. Therefore, the isotopic composition of the BaCO<sub>3</sub> samples reflect those of DCP at the time of precipitation (*i.e.*,  $\delta^{18}O_{BaCO3} = \delta^{18}O_{DCP}$  and  $\Delta_{47~BaCO3} = \Delta_{47~DCP}$ ).

Over the course of isotopic equilibration,  $\delta^{18}O_{DCP}$  asymptotically increased from the first/lowest value (ranging from -14.5% to -12.5%) to about -3.8% and plateaued thereafter in all of the experimental series. This is displayed in Fig. 3b and Fig. 4beh, in which the  $\delta^{18}O$  data are expressed as apparent fractionations with respect to  $H_2O$  ( $^{18}\epsilon_{DCP-H2O}$ , Eqs. (9) and (10)). For all of the experimental series,  $^{18}\epsilon_{DCP-H2O}$  at the initial and equilibrium condition is consistent with what is expected from  $\delta^{18}O$  of the experimental NaHCO<sub>3</sub> and the theoretical prediction shown in Fig. 1b that is based on Zeebe (2007). Also note that the time needed for DCP to reach the well-defined  $^{18}$ - $\epsilon_{DCP-H2O}$  plateau (*i.e.*, equilibrium) progressively decreased in response to an increase in the amount of CA added to the experimental series (see Fig. 4beh).

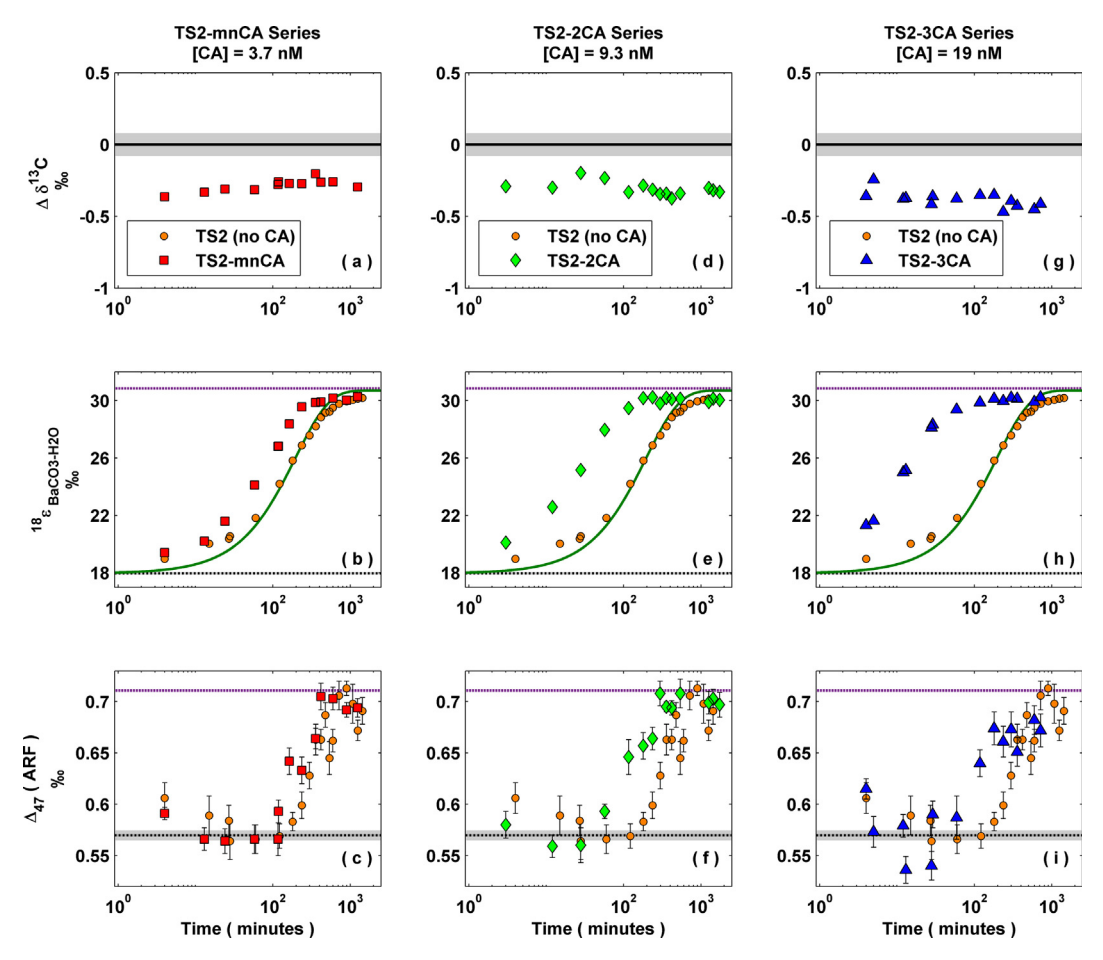


Fig. 4. Summary of isotope data from the experimental series performed with the enzyme carbonic anhydrase (CA). Isotope data are displayed in the same manner as Fig. 3. For the  $^{18}\epsilon_{BaCO3-H2O}$  and  $\Delta_{47}$  profiles (middle and bottom panels), the data from the TS2 experimental series (normal/uncatalyzed isotopic equilibration) are also displayed for comparison. The error bars for the isotope data are  $\pm$  1SE.

The overall trajectory of  $\Delta_{47}$  equilibration in DCP traced by the BaCO3 samples was clearly different from those of  $\delta^{18}$ O. In the TS2 series with no CA addition,  $\Delta_{47}$  of DCP dropped from 0.606% to 0.564% in the first ~30 minutes and subsequently rose to 0.700% by ~900 minutes and remained fairly constant afterwards (Fig. 3c). In the TS2mnCA series with [CA] = 3.7 nM,  $\Delta_{47}$  of DCP similarly decreased from 0.591% to 0.564% within the first ~30 minutes, rebounded to about 0.700% by ~420 minutes and then plateaued (Fig. 4c). In the TS2-2CA series with [CA] = 9.3 nM,  $\Delta_{47}$  of DCP quickly dropped from 0.580% to about 0.560% within the first ~15 minutes and then increased and plateaued at about 0.701% by ~300 minutes (Fig. 4f). Note that  $\Delta_{47}$  of the well-defined plateau at ~0.700% in these experimental series are consistent with the theoretical prediction at pH 8.9 (Fig. 1d).

However, the results from the TS2-3CA series with [CA] = 19 nM were somewhat anomalous. Specifically,  $\Delta_{47}$  values measured on two sets of replicate samples (precipitated only 1–2 minutes apart) situated in the early part of the time-series did not reproduce well (Fig. 4i). This makes the overall trajectory somewhat unclear, though the initial decline in  $\Delta_{47}$  of DCP is still evident. As seen

in other experimental series, DCP for the TS2-3CA series eventually plateaued at ~0.660‰. But this level is lower than the expected equilibrium by ~0.040‰.

In summary,  $\Delta_{47}$  equilibration in DCP initially proceeds to even stronger disequilibrium before its subsequent approach towards equilibrium, resulting in a characteristic "dip" in the  $\Delta_{47}$  equilibration trajectory in all of our experimental series. Moreover, our datasets suggest an acceleration of  $\Delta_{47}$  equilibration in DCP in response to an increase in the amount of CA added to the system, despite some noise in our experimental data.

## 4. DISCUSSION

#### 4.1. Analytical considerations

Our newly measured  $\delta^{13}C$  and  $\delta^{18}O$  values of the BaCO<sub>3</sub> sample did not agree perfectly with the original UZ12 data. While  $\delta^{13}C$  values measured at Caltech were persistently off by ~0.3% relative to the original values reported in UZ12, the  $\delta^{18}O$  offsets were larger and more variable (Fig. 2a). We first emphasize that the observed inconsistency in the isotope data between the present study and UZ12 should nei-

ther undermine the quality of our data nor hinder our data interpretation. This is because (#1)  $\delta^{13}C$  of BaCO<sub>3</sub> show no temporal drift and agree well with  $\delta^{13}C$  of the experimental NaHCO<sub>3</sub>, (#2) the extent of the  $\delta^{18}O$  offsets is small compared to the overall changes in  $\delta^{18}O$  of BaCO<sub>3</sub> over time (~1.5‰ at most vs. over 10‰) and (#3) the analytical uncertainty and the noise in our  $\Delta_{47}$  data are unrelated to the  $\delta^{18}O$  offsets (they are largely due to operating conditions of the instrument).

Nonetheless, the  $\delta^{18}$ O offsets spanning over -1.5%to  $\pm 0.6\%$  warrant some discussion. Although the  $\delta^{18}$ O offsets appear non-systematic in Fig. 2a, these offsets from all experimental series show the same general pattern when they are plotted against  $\delta^{18}$ O values of the BaCO<sub>3</sub> samples (Fig. 2b). The Caltech-based  $\delta^{18}$ O values are systematically more negative for the BaCO<sub>3</sub> samples having higher  $\delta^{18}$ O values and more positive for the samples with lower  $\delta^{18}$ O than the UZ12's original data generated at UCSC. In other words, the Caltech-UCSC δ<sup>18</sup>O offsets are directly related to the sample  $\delta^{18}O$  values. We note that, at Caltech, the measurements were standardized by using a wellcalibrated reference gas. At UCSC, data standardization was done by a two-point correction using the NBS-18 reference material and an externally-calibrated in-house carbonate standard analyzed with samples. It is possible that such a difference in the data standardization practice (i.e., calibration slopes) played a role for the  $\delta^{18}$ O offsets, as our BaCO<sub>3</sub> samples cover a relatively wide  $\delta^{18}$ O range. As opposed to the BaCO<sub>3</sub> samples, the Caltech-based  $\delta^{18}$ O for the experimental NaHCO<sub>3</sub> agree with the UZ12. Also, analyses on the NBS-19 reference material and other carbonate standards at Caltech were consistent with their accepted values. Thus, the issue discussed here seems to apply to BaCO<sub>3</sub> only, for which we cannot rule out an additional possibility of laboratory-specific biases and/or isotope fractionations during the acid digestion of BaCO<sub>3</sub>. For instance, differences in the reaction time and/or temperature of the acid digestion between each laboratory can be important factors.

The  $\Delta_{47}$  analytical uncertainty ranged from  $\pm 0.005$ to  $\pm$  0.021‰ (1 $\sigma$ ), with an average of  $\pm$  0.014‰. The error bounds bracketing some of the  $\Delta_{47}$  data-points hence can be up to  $\pm$  0.04‰, which is almost as large as the signal of the non-first-order  $\Delta_{47}$  equilibration kinetics (i.e., the magnitude of the dip, Fig. 3 and Fig. 4). Despite the data uncertainties, our  $\Delta_{47}$  equilibration trajectories follow the same general pattern similar to SS18. However, one exception to this statement is the TS2-3CA  $\Delta_{47}$  dataset, which was generated in November, 2019 (all other samples were analyzed in October-November, 2018). The  $\Delta_{47}$  data show more significant noise for the first ~30 minutes of equilibration, as the replicate samples prepared only ~1-2 minutes apart from the same NaHCO<sub>3</sub> solutions resulted in a  $\Delta_{47}$ difference exceeding 0.04% (Fig. 4i). Also, the  $\Delta_{47}$  value at which the equilibration trajectory plateaued was oddly ~0.03‰ lower than the expected equilibrium. As these inconsistencies are likely due to instrument instability during the analytical sessions in 2019, less weight will be given to the TS2-3CA series in the following data interpretation.

#### 4.2. Overview of the experimental results

Our new experimental data are in good agreement with SS18. Equilibration of  $\delta^{18}O$  in DCP traces an asymptotic path that can be modeled by a simple first-order exponential decay function (Beck et al., 2005; UZ12; SS18; Weise and Kluge, 2020). In contrast,  $\Delta_{47}$  equilibration initially trends toward even stronger disequilibrium before a subsequent rebound and continuous increase toward the expected equilibrium, which is manifested as the prominent "dip" in the early phase of equilibration (Fig. 3c). This is exactly the non-first-order behavior reported by SS18 (Fig. S1c). Our data further demonstrate that the combination of the first-order kinetics for  $\delta^{18}O$  equilibration and the non-first-order kinetics for  $\Delta_{47}$  equilibration also holds in the presence of the CA enzyme (Fig. 4).

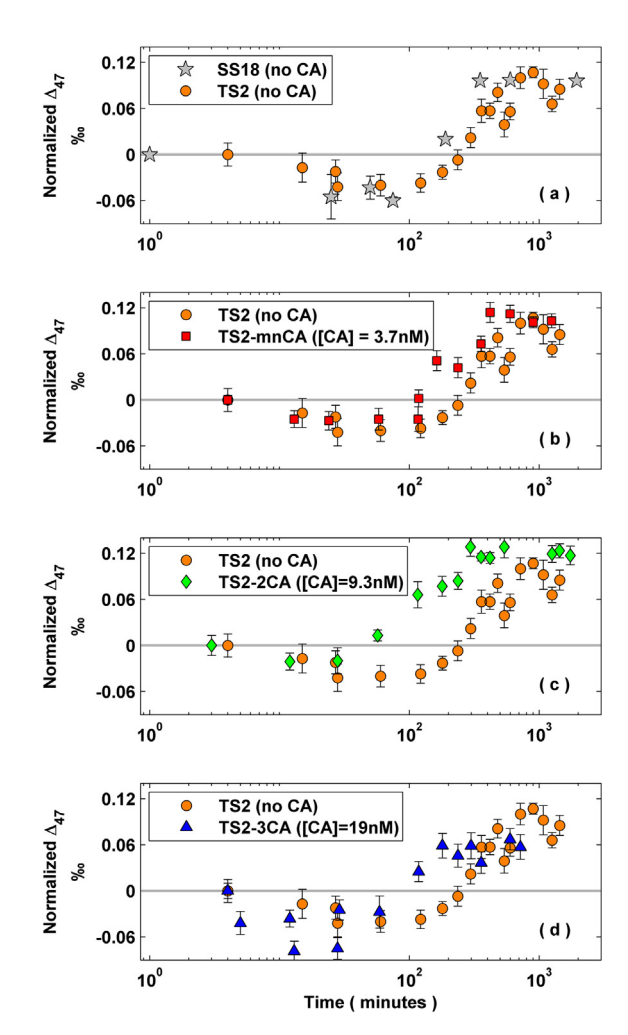


Fig. 5. Time-series  $\Delta_{47}$  data normalized to the first data-point in each series. (a) Comparison of uncatalyzed  $\Delta_{47}$  equilibration trajectory based on SS18 25 °C data and our TS2 experimental series. (b) Comparison of uncatalyzed TS2 experimental series and TS2-mnCA series, to which 3.7 nM of CA enzyme was added. (c) Comparison with TS2-2CA series, to which 9.3 nM of CA enzyme was added. (d) Comparison with TS2-3CA series, to which 19 nM of CA enzyme was added.

The  $\Delta_{47}$  data from our TS2 experimental series and the SS18 25 °C experiments (both under normal condition without CA enzyme) can be directly compared after normalizing the  $\Delta_{47}$  data to the first data-point in each timeseries (Fig. 5a). This comparison shows a similar magnitude of the dip in the  $\Delta_{47}$  equilibration trajectory between our TS2 and SS18's data. Moreover, when the dip is compared between our TS2 series and other enzymatically-catalyzed series (Fig. 5), the observed differences in its magnitude are small and, for the most part, within the analytical uncertainty (though slightly controversial for the TS2-3CA dataset). In other words, the magnitude of the dip is fairly uniform regardless of the presence and concentration of CA. However, CA affects how quickly the system comes out of the dip and eventually reaches  $\Delta_{47}$  equilibrium. Our results thereby confirm that CA accelerates not only  $\delta^{18}$ O but also  $\Delta_{47}$  equilibration in DCP.

For the TS2, TS2-mnCA and TS2-2CA series, equilibrium  $^{18}$  $\epsilon_{DCP-H2O}$  and  $\Delta_{47}$  of DCP are consistent at about 30% and 0.700%, respectively. These agree well with the theoretical prediction ( $^{18}\epsilon_{\mathrm{DCP-H2O}}^{\mathrm{EQ}}=30.70\pm0.24\%$  and  $\Delta_{47}^{\rm EQ} = 0.708 \pm 0.002\%$ , see Fig. 1) at our experimental pH<sub>NBS</sub> of 8.9 (Fig. 4). In contrast, the  $\delta^{18}$ O and  $\Delta_{47}$  equilibrium values in SS18's data at 25 °C ( $^{18}\varepsilon_{DCP-H2O} \approx 28.56\%$ and  $\Delta_{47} \approx 0.644\%$ , which are the average of the last three time-series data points, see Fig. S1c) are lower than the theoretical prediction at their experimental  $pH_{NBS}$  range of 9.2 to 9.4 ( $^{18}\epsilon_{DCP-H2O}^{EQ} = 29.9$  to 30.3% and  $\Delta_{47}^{EQ} = 0.701$  to 0.705‰, see Fig. 1). Roughly 1.4‰ of <sup>18</sup>O depletion relative to the expected equilibrium can be explained by the choice of AFF for  $\delta^{18}$ O. We notice that SS18 applied the BaCO<sub>3</sub>specific AFF by Böttcher (1996). But this is not the case in the quantitative BaCO<sub>3</sub> precipitation experiments of Uchikawa and Zeebe (2013) upon which the theoretical prediction shown in Fig. 1 is based (the BaCO<sub>3</sub> samples were treated as calcite and no corrections with BaCO<sub>3</sub>-specific AFF were made). If handled equally as calcite (e.g., UZ12),  $\delta^{18}$ O of the BaCO<sub>3</sub> samples by SS18 should increase by 1.12‰ at their acid digestion temperature of 90 °C. This largely resolves the offset between experimental and theoretical  $^{18}\epsilon_{\mathrm{DCP-H2O}}^{\mathrm{EQ}}$  in SS18's data. However, the equilibrium  $\Delta_{47}$  value being lower than the theoretical prediction by ~0.060% in the SS18 data cannot be explained by the choice of the AFF, because all of the  $\Delta_{47}$  data discussed here, including ours, SS18 and Tripati et al. (2015) that was used for our theoretical calculation (Fig. 1) are based on the CaCO<sub>3</sub>-specific  $\Delta_{47}$  AFF. Thus, this inconsistency calls for an alternative explanation (to be further discussed in Section 4.3.1).

Lastly, we discuss the very first data point in the TS2 time-series (Fig. 3), which was precipitated only 4 minutes after the NaHCO<sub>3</sub> powder was dissolved into H<sub>2</sub>O. With such a short equilibration time (and without catalytic influence of CA), there should be a decent isotopic agreement between this particular BaCO<sub>3</sub> sample and the experimental NaHCO<sub>3</sub> ( $\delta^{18}$ O<sub>VPDB</sub> =  $-15.63 \pm 0.06\%$  and  $\Delta_{47} = 0.570 \pm 0.005\%$ ). But the isotopic values measured on this sample are slightly higher ( $\delta^{18}$ O<sub>VPDB</sub> = -14.48% and  $\Delta_{47} = 0.606\%$ ). The more positive  $\delta^{18}$ O value for BaCO<sub>3</sub> over NaHCO<sub>3</sub> is in line with the direction of  $\delta^{18}$ O equilibra-

tion, where  $\delta^{18}O$  of DCP increases over time (Fig. 3b). Thus, the  $\delta^{18}O$  offset between this BaCO<sub>3</sub> sample and the experimental NaHCO<sub>3</sub> can be explained by partial equilibration. In contrast,  $\Delta_{47}$  of DCP decreased during the initial phase of equilibration (Fig. 3c). Thus, the positive  $\Delta_{47}$  offset in DCP relative to NaHCO<sub>3</sub> is against the direction of equilibration. This may stem from a potential difference in  $\Delta_{47}$  AFF between BaCO<sub>3</sub> and NaHCO<sub>3</sub>. While some constraints of AFF were made on BaCO<sub>3</sub> (Guo et al., 2009; Tripati et al., 2015), NaHCO<sub>3</sub>-specific  $\Delta_{47}$  AFF has yet to be investigated. Alternatively, there may be hitherto unrecognized  $\Delta_{47}$  effects upon a rapid dissolution/ionization of NaHCO<sub>3</sub> in H<sub>2</sub>O.

## 4.3. Data interpretation with the SS18 model

# 4.3.1. Uncatalyzed $k_{46}$ , $k_{47}$ and $^{13-18}KIE$

Reevaluation of SS18's data at 25 °C by our optimized modeling approach led to  $^{13-18}$ KIE = 0.980, or a ~20% isotope effect. But we note a few caveats in their experimental data: (#1) pH<sub>NBS</sub> of their NaHCO<sub>3</sub> solution changed from 9.2 to 9.4 over the course of their experiment, (#2)  $\delta^{13}$ C of DCP recorded by their BaCO<sub>3</sub> samples increased with time by ~2.5% (Fig. S1a), (#3)  $\delta^{18}$ O equilibration in DCP outpaced the time-course predicted by the theoretical prediction following UZ12 (Fig. S1b), and (#4)  $\Delta_{47}$  of DCP plateaued at ~0.06% lower than the expected equilibrium (Fig. S1c). In their approach, from 1 L of NaHCO<sub>3</sub> solution, 20 mL of the solution were recurrently withdrawn to perform BaCO<sub>3</sub> precipitation over the course of equilibration (a total of 240 mL withdrawal for 12 samples). The changes in solution pH and  $\delta^{13}$ C of DCP described above (items #1 and #2) suggest CO2 degassing induced by continuous increase in the headspace (Mook, 1986; Zhang et al., 1995; Zeebe and Wolf-Gladrow, 2001). Items #3 and #4 also seem to support CO<sub>2</sub> degassing. Affek and Zaarur (2012) showed that CO<sub>2</sub> degassing leads to an increase in  $\delta^{18}$ O but a decrease in  $\Delta_{47}$  of the remaining DCP. This may introduce some uncertainties in the rate constants  $k_{46}$  and  $k_{47}$ , and thus <sup>13-18</sup>KIE derived from SS18's experimental data. For instance,  $k_{46}$  derived from their data is  $10.03 \times 10^{-3} \text{ min}^{-1}$ , which is sizably higher than the  $\delta^{18}O$  equilibration rate constant  $\tau^{-1}$  at their experimental pH<sub>NBS</sub> of 9.2 to 9.4 (3.83  $\times$  10<sup>-3</sup> to 4.24  $\times$  10<sup>-3</sup> min<sup>-1</sup>). Moreover, the theory predicts that the rate constant  $\tau^{-1}$  to decrease with pH (Fig. 1c). But  $k_{46}$  derived from the SS18 data is almost twice the value constrained from our TS2 data performed at pH<sub>NBS</sub> 8.9.

The issue of  $CO_2$  degassing should be negligible in our experiments, as the NaHCO<sub>3</sub> solutions were sealed into individual bottles with minimal headspace (UZ12). This is validated by the close  $\delta^{13}C$  agreement between the BaCO<sub>3</sub> samples and NaHCO<sub>3</sub> as well as the lack of drift in  $\delta^{13}C$  of BaCO<sub>3</sub> with time (Fig. 3a). And, as expected, there is a much better agreement between  $k_{46}$  derived from our TS2 data and the theoretically predicted  $\tau^{-1}$  from UZ12 (see Table 1). By assigning <sup>13-18</sup>KIE = 0.978 and  $\delta^{18}O_{C13}^{EQ} = -3.02\%$ , the optimized SS18 model was able to replicate the dip in the  $\Delta_{47}$  equilibration trajectory for our TS2 data (Fig. 6 and Fig. S4).

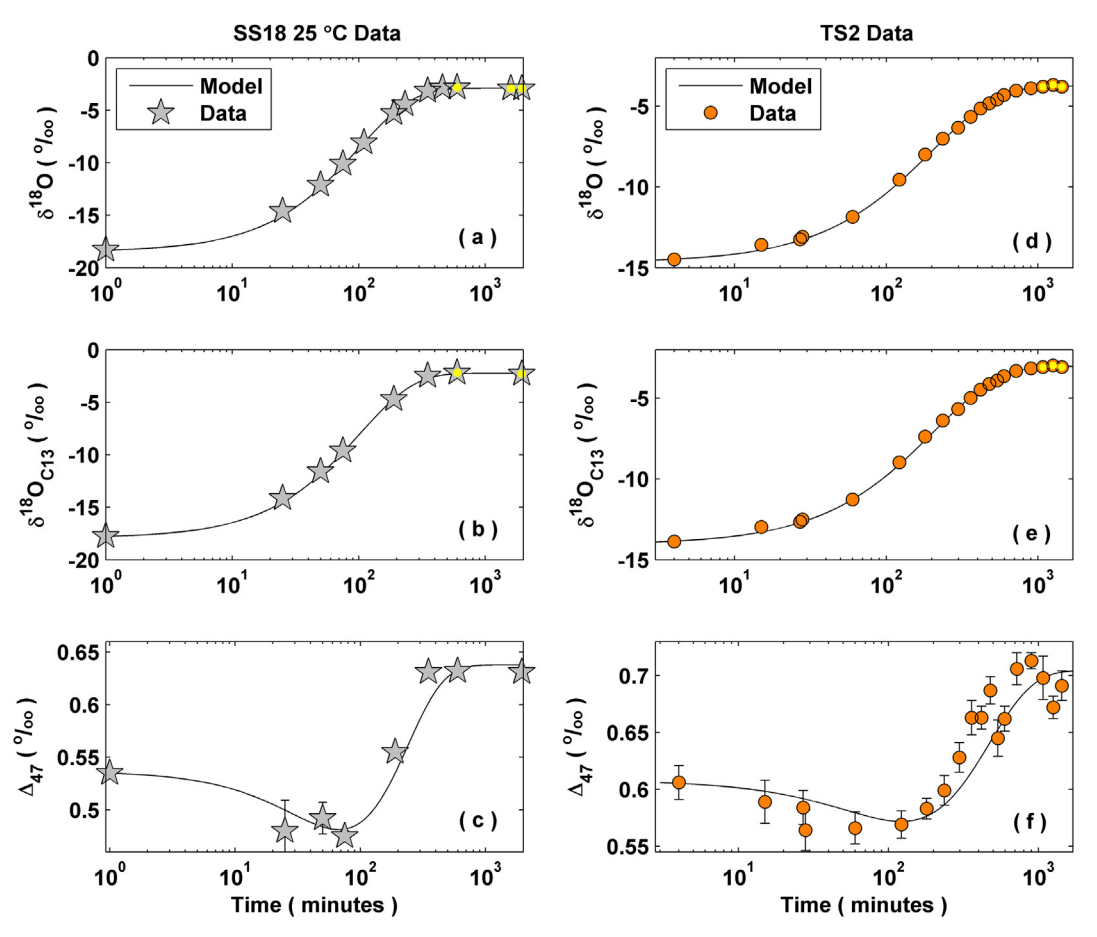


Fig. 6. Application of the optimized SS18 model to the SS18 25 °C and our TS2 data (normal/uncatalyzed isotopic equilibration). (a)  $\delta^{18}$ O of DCP, (b)  $\delta^{18}$ O<sub>C13</sub>, which is  $\delta^{18}$ O of oxygen bound to  $^{13}$ C isotope in DCP (as defined by SS18) and (c)  $\Delta_{47}$  of DCP. The modeling results shown here represent the best-fit to the experimental  $\Delta_{47}$  data. The quantity  $\delta^{18}$ O<sub>C13</sub> was iteratively estimated from  $\delta^{13}$ C,  $\delta^{18}$ O and  $\Delta_{47}$  measured on the BaCO<sub>3</sub> samples. The data-points marked with yellow dots (panels a-e) were averaged to define equilibrium  $\delta^{18}$ O and  $\delta^{18}$ O<sub>C13</sub> values to be used for exponential data fitting in the model (detailed in Section 2.3.1).

By replacing  $\tau$  in Eq. (5) with the reciprocal of  $k_{46}$ ,  $T_{EQ}$ for δ<sup>18</sup>O equilibration is ~920 minutes at our experimental pH<sub>NBS</sub> of 8.9. In comparison,  $T_{EQ}$  for  $\Delta_{47}$  equilibration is predicted to be  $\sim$ 940 minutes by replacing  $\tau$ with the reciprocal of  $k_{47}$ . A difference of  $\sim 20$  minutes between  $T_{EO}$  for  $\delta^{18}$ O and  $\Delta_{47}$  equilibration is too short to be resolved by the typical sampling of our BaCO<sub>3</sub> precipitation experiments (also the case in SS18), which is typically coarse in the equilibrium tail of the timeseries. While the effect is rather small in terms of equilibration timescales, the difference between  $k_{46}$  and  $k_{47}$ apparently leads to a profound non-first-order characteristic in the  $\Delta_{47}$  equilibration trajectory. Also note that, as described in Section 2.3.1,  $^{13\text{-}18}\text{KIE}$  is a measure of the difference in  $^{12}\text{C}$  and  $^{13}\text{C}$  exchange rate for transformation of <sup>18</sup>O-substituted CO<sub>2(aq)</sub> to dissolved carbonate species  $(286_{(aq)} \rightarrow 2866 \text{ vs. } 386_{(aq)} \rightarrow 3866) \text{ via Eq. (3)}$ and Eq. (4). Likewise, carbon isotope KIFs for  $CO_2$  hydration and hydroxylation ( $^{13}\alpha_{k_{+1}}^{KIF}=k_{+1}/^{13}k_{+1}$  and  $^{13}\alpha_{k_{-4}}^{KIF} = k_{+4}/^{13}k_{+4}$ , Eq. (17)–(20)) reflect the difference in 12C and 13C exchange rate, but for unsubstituted species in oxygen  $(266_{(ag)} \rightarrow 2666 \text{ vs. } 366_{(ag)} \rightarrow 3666)$ . Thus,

it is not surprising that the inverse of  $^{13\text{-}18}\text{KIE} (= k_{46}/k_{47} = (0.975)^{-1} = 1.026)$  determined from our experimental data is similar in magnitude to  $^{13}\alpha_{k_{+1}}^{KIF}$  and  $^{13}\alpha_{k_{+4}}^{KIF}$  reported in the literature (see Section 4.4.1).

# 4.3.2. Enzymatically-catalyzed $k_{46}$ , $k_{47}$ and $^{13-18}KIE$

 $CO_2$  hydration is a critical pathway that allows direct exchange of oxygen isotopes between DIC species and  $H_2O$ . Since its reaction rate is much slower than other reactions occurring in the dissolved carbonate system,  $CO_2$  hydration represents a major bottleneck for  $\delta^{18}O$  equilibration in DCP (Zeebe and Wolf-Gladrow, 2001). Enzymatic catalysis of  $CO_2$  hydration by CA effectively accelerates  $\delta^{18}O$  equilibration in DCP (UZ12). Our newly generated isotope data not only verify this notion but also demonstrate that CA likewise accelerates  $\Delta_{47}$  equilibration (Fig. 4).

Our optimized modeling scheme is able to trace the  $\delta^{18}O$  and  $\Delta_{47}$  equilibration trajectories reflected by the TS2-mnCA, TS2-2CA and TS2-3CA experimental series that were conducted at different CA concentrations (Fig. 7). We find that  $k_{46}$  increases almost linearly with concentrations of CA added to each experimental series (Fig. 8),

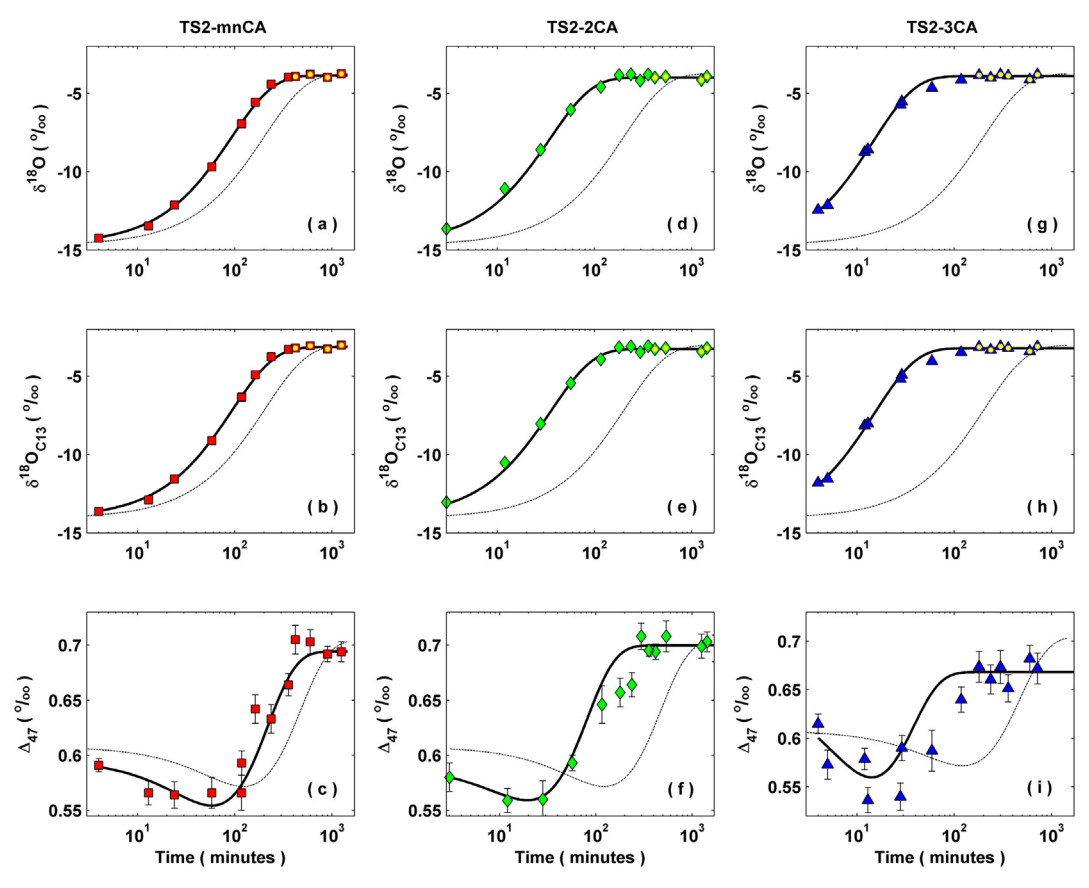


Fig. 7. Application of the optimized SS18 model to the isotope data from our CA experiments (TS2-mnCA, TS2-2CA and TS2-3CA). Modeling results and isotope data are displayed in the same fashion as Fig. 6. Also shown here is the modeling output for TS2 experiments as a reference for normal/uncatalyzed isotopic equilibration (dotted curve).

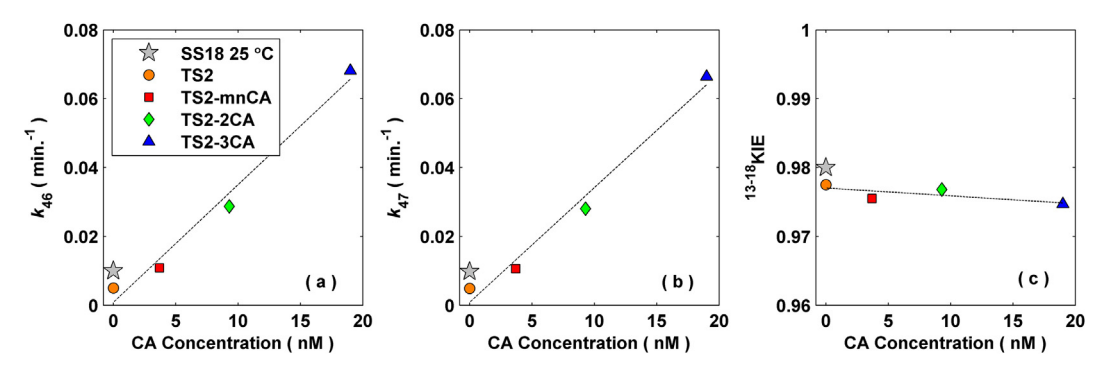


Fig. 8. Display of  $k_{46}$ ,  $k_{47}$  and  $^{13-18}$ KIE (see Eq. (13)–(15)) determined from the optimized SS18 model for all of the experimental series examined in this study. Note that  $k_{46}$  and  $k_{47}$  linearly increases with CA concentrations (**a** and **b**), while there is no robust trend as a function of CA concentrations for  $^{13-18}$ KIE (**c**). The slope of the linear regression (dashed line) on  $k_{46}$ ,  $k_{47}$  and  $^{13-18}$ KIE as a function of CA concentration was  $3.41 \times 10^{-3}$  ( $r^2 = 0.982$ ),  $3.33 \times 10^{-3}$  ( $r^2 = 0.982$ ) and  $-1.12 \times 10^{-4}$  ( $r^2 = 0.546$ ), respectively.

which agrees with the formulation of the overall CO<sub>2</sub> hydration rate constant as a function of CA based on Michaelis-Menten kinetics by UZ12 (see Eq. (21) and Fig. 9 therein). In contrast, <sup>13-18</sup>KIE values determined from SS18 model fit to our experimental data are almost uniform at ~0.976 for all of the CA-catalyzed cases (Table 1, Fig. 8). This is in line with a fairly similar magnitude of the

dip in the  $\Delta_{47}$  equilibration trajectory for all of our experimental series, regardless of the presence and concentration of CA (Fig. 5). It follows that, within the range tested here, CA only reduces the time required for  $\Delta_{47}$  equilibrium in DCP without altering the non-first-order characteristics in the equilibration trajectory (*i.e.*, the ratio of  $k_{46}$  and  $k_{47}$  remains constant).

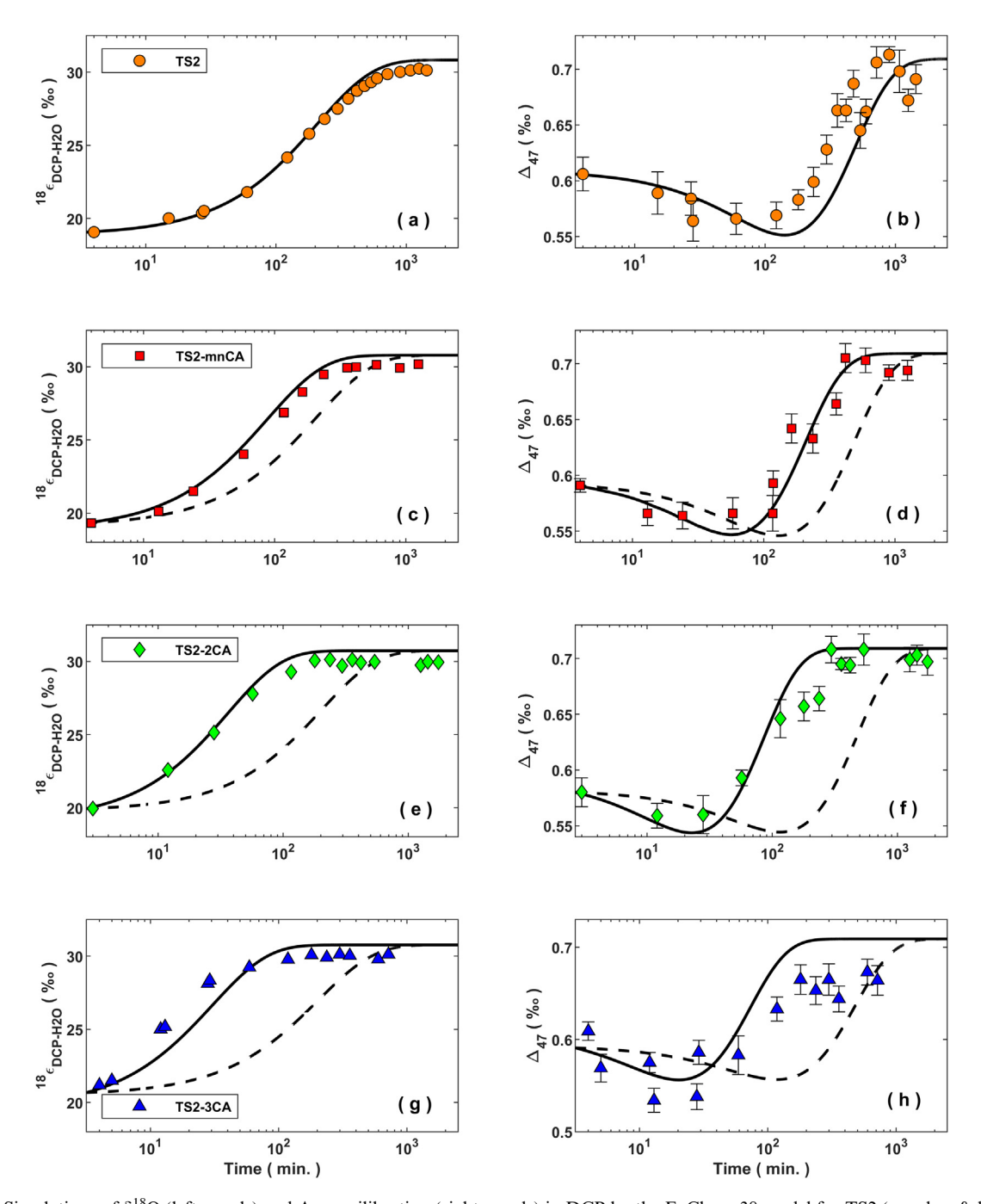


Fig. 9. Simulations of  $\delta^{18}O$  (left panels) and  $\Delta_{47}$  equilibration (right panels) in DCP by the ExClump38 model for TS2 (panels a & b), TS2-mnCA (panels c & d), TS2-2CA (panels e & f) and TS2-3CA (panels g & h) experimental condition. Dotted curves (displayed in panels c to h) mark the model simulation for TS2 experimental condition for a comparison to the normal/uncatalyzed isotopic equilibration without CA enzyme.

# 4.4. Data interpretation with the ExClump38 model

## 4.4.1. Sensitivity test

The differential equations solved in the ExClump38 model are set up as a function of equilibrium constants (K's), kinetic rate constants (K's), equilibrium fractionation factors ( $^{13}\alpha^{EQ}$ 's and  $^{18}\alpha^{EQ}$ 's) and kinetic carbon and oxygen KIFs ( $^{13}\alpha^{KIF}$ 's and  $^{18}\alpha^{KIF}$ 's) and intrinsic kinetic clumped isotope effects ( $^{47}$ KIE's). We follow Guo (2020) for the

definition of <sup>47</sup>KIE's associated with Eq. (25) to Eq. (28), and they depend on KIFs specific to the clumped species ( $^{47}\alpha^{\rm KIF}$ 's) in addition to more conventional  $^{13}\alpha^{\rm KIF}$ 's and  $^{18}\alpha^{\rm KIF}$ 's for hydration and hydroxylation (see the full model description in Supplementary Materials). Note that  $^{47}$ KIE's by Guo (2020) are fundamentally different from  $^{13-18}$ KIE defined by SS18 (Eq. (28)). As explained in Section 4.3.1,  $^{13-18}$ KIE by SS18 simply reflects the subtle difference in the rate of change in [2866] and [3866] in DCP as singly-

and doubly-substituted CO<sub>2</sub> (286 and 386, respectively) undergo hydration and hydroxylation.

Of the isotope fractionations listed above, <sup>13</sup>α<sup>KIF</sup>,s,  $^{18}\alpha^{\rm KIF}$ 's and  $^{47}{\rm KIE}$ 's are treated as adjustable parameters because experimental/theoretical constraints on them are either limited or inconsistent across different studies in some cases (e.g., Zeebe, 2014; Guo and Zhou, 2019; Guo, 2020; Yumol et al., 2020). We first performed sensitivity runs to address the impact of these adjustable parameters on the model outcome. Each parameter was individually varied from 0.990 to 1.015 (over 25‰), while others were fixed at a value of 1 (i.e., no additional fractionations). The results show that the non-first-order characteristics in the  $\Delta_{47}$  equilibration trajectory (i.e., the dip) only arises when carbon isotope KIFs and intrinsic clumped isotope effects associated with Eq. (19), Eq. (20), Eq. (25) and Eq. (27)  $(^{13}\alpha_{k_{+1}}^{KIF}, ^{13}\alpha_{k_{+4}}^{KIF}, ^{47}\text{K}\text{IE}_{p+1})$  and  $^{47}\text{K}\text{IE}_{p+4})$  are in effect (Figure S5). This corroborates SS18 that the  $\Delta_{47}$  equilibration trajectory is fundamentally shaped by <sup>13-18</sup>KIE, which is essentially the same as carbon isotope KIF for conversion of CO<sub>2</sub> to dissolved carbonate species, only except the fact that CO<sub>2</sub> is <sup>18</sup>O-substitued in this case (see Section 4.3.1). In contrast, all of  $^{18}\alpha^{KIF}$ 's (for Eq. (21) to Eq. (24)) and <sup>47</sup>KIE's associated with Eq. (26) and Eq. (28) had hardly any influence on the model output. Thus, for the ExClump38 model, we directly used the estimates by Guo and Zhou (2019) and Guo (2020) for these particular <sup>18</sup>α<sup>KIF</sup>'s and <sup>47</sup>KIE's.

The values for  ${}^{13}\alpha_{k_{+1}}^{KIF}, {}^{13}\alpha_{k_{+4}}^{KIF}, {}^{47}\text{KIE}_{p+1}$  and  ${}^{47}\text{KIE}_{p+4}$ require more careful considerations, as they are critical for the modeling outcome (Figure S5). Guo (2020) developed a numerical model IsoDIC for simulating the evolution of a suite of clumped species in DCP (i.e., mass 63, 64 and 65 signals), which was able to reproduce the timeseries  $\delta^{18}$ O and  $\Delta_{47}$  data of SS18 (see Fig. 9a therein). For this work, Guo also conducted theoretical calculations and provided estimates of -0.146% and -0.016% for  ${}^{47}\text{KIE}_{p+1}$  and  ${}^{47}\text{KIE}_{p+4}$ , respectively. We are not aware of other studies that attempted to constrain these clumped isotope effects. This makes it difficult to further evaluate Guo's values. However, our sensitivity runs indicate that, even if those values were off by 1%, the consequence on the modeled  $\Delta_{47}$  equilibration trajectory would be relatively small (see Fig. S5gh). We hence relied on the values of Guo (2020) in the ExClump38 model.

In terms of carbon isotope KIF for CO<sub>2</sub> hydroxylation, experimental and field data from independent studies point to relatively consistent  $^{13}$ C depletion of about 17‰ in the resultant HCO<sub>3</sub> between ~20 to ~30 °C (Clark et al., 1992; Falk et al., 2016; Christensen et al., 2021), or  $^{13}\alpha_{k_{+4}}^{KIF}$  of 1.0170. In terms of carbon isotope KIF for CO<sub>2</sub> hydration, the results from a recent experimental study by Yumol et al. (2020) indicate ~17.6‰ of  $^{13}$ C depletion in the resultant HCO<sub>3</sub>  $^{13}\alpha_{k_{+1}}^{KIF}$  = 1.0176). As this is higher than the  $^{13}\alpha_{k_{+1}}^{KIF}$  from prior experimental studies (Marlier and O'Leary, 1984; O'Leary et al., 1992; Clark and Lauriol, 1992), they argued that the value of 1.0176 is likely the closest to the true extent of carbon isotope KIF of CO<sub>2</sub> hydration. With the input of  $^{13}\alpha_{k_{+1}}^{KIF}$  = 1.0170 and  $^{13}\alpha_{k_{+1}}^{KIF}$  = 1.0176,

the ExClump38 model nicely reproduces the overall trajectory of  $\Delta_{47}$  equilibration in DCP and, importantly, the magnitude of the  $\Delta_{47}$  dip observed in our TS2 experimental data (Fig. 9ab). Note that these KIFs have also been investigated via theoretical calculations (Guo, 2009; Zeebe, 2014; Guo 2020; Boettger and Kubicki, 2021), and some of those predict larger values. For the ExClump38 model, however, we rely on the observational constraints described above. This is because theoretical calculations depend heavily on the assumed conditions and reaction pathways or mechanisms (see Zeebe, 2014) and thus the estimates within in a single study and across independent studies can vary significantly (e.g., Zeebe, 2014; Boettger and Kubicki, 2021).

# 4.4.2. <sup>13</sup>KIF for CO<sub>2</sub> hydration mediated by CA enzyme?

Provided with all the input parameters and constants, the ExClump38 model can replicate the overall patterns of the  $\delta^{18}O$  and  $\Delta_{47}$  equilibration trajectory represented by our TS2 experimental dataset (Fig. 9ab). In addition, as shown in Fig. 9c-h, the model is capable of simulating the equilibration time-course for DCP with CA enzyme (TS2-mnCA, TS2-2CA and TS2-3CA datasets), which only requires the CA rate enhancement factor to be equally applied to all of the CO<sub>2</sub> hydration rate constants ( $k_{\pm 1}$ ,  $k_{\pm 1}$ ,  $a_{\pm 1}$ ,  $b_{\pm 1}$ ,  $p_{\pm 1}$  and  $s_{\pm 1}$ , see Section 2.3.2) without additional fractionation by CA itself (Chen et al., 2018).

The sensitivity analyses conducted on the ExClump38 model (Section 4.4.1) indicated that the two major parameters responsible for the non-first-order characteristics (i. e., the dip) in the  $\Delta_{47}$  equilibration kinetics is carbon isotope KIFs for CO<sub>2</sub> hydration and hydroxylation (Fig. S5). This leads us to the experimental studies by O'Leary and colleagues (Marlier and O'Leary, 1984; Paneth and O'Leary, 1985; O'Leary et al., 1992). Marlier and O'Leary (1984) conducted two types of experiments at 24 °C. First, HCO<sub>3</sub> derived from CO<sub>2(g)</sub> via dissolution and subsequent hydration was rapidly converted to malate by using some enzymes. Second, CO<sub>2(g)</sub> was rapidly evolved from NaHCO3 solution via dehydration and subsequent degassing using an inert gas. After isotopic analyses of the reaction products, they concluded 13 aKIF for CO2 hydration and HCO<sub>3</sub> dehydration to be 1.0069 and 1.0147 (or 6.9% and 14.7%), which broadly agrees with  $^{13}\alpha^{EQ}_{HCO_{2}^{-}-CO2(g)}$  of 1.0080 at 24 °C by Zhang et al., (1995) (see Eq. A42 in the Supplementary Materials).

Paneth and O'Leary (1985) repeated the degassing experiments, but with CA enzyme in the NaHCO<sub>3</sub> solution, and found  $^{13}\alpha^{\rm KIF}$  of 1.0101 for HCO<sub>3</sub> dehydration in this case. Then, by assuming no CA effect on the equilibrium fractionation factor (see UZ12 for the case of oxygen isotopes) and with  $^{13}\alpha^{EQ}_{\rm HCO_3^--CO2(g)}$  of Zhang et al. (1995),  $^{13}\alpha^{\rm KIF}$  for CA-catalyzed CO<sub>2</sub> hydration becomes 1.001. The difference in their experimental outcome ( $^{13}\alpha^{\rm KIF}$  of 1.0069 vs. 1.001) intuitively implies that CA lowers carbon isotope KIF for CO<sub>2</sub> hydration ( $^{13}\alpha^{\rm KIF}_{k+1}$ ). If this is really the case, from our sensitivity analyses with the ExClump38 model (Fig. S5a), the dip in the  $\Delta_{47}$  equilibration trajectory is expected to shoal in response to CA additions. Yet, our data do not clearly show such a trend (Fig. 5). Though

we are unable to provide compelling explanation(s) for this, a few possibilities can be explored.

If  $^{13}\alpha_{k+1}^{KIF}$  indeed changes with CA (Marlier and O'Leary, 1984; Paneth and O'Leary, 1985), it is possible that the signal was not adequately captured in our experiments, potentially because the analytical uncertainty and the noise in our  $\Delta_{47}$  were too large and/or the CA concentrations were too low (refer to Section 4.1. for the issues in our TS2-3CA dataset with the highest CA concentration). Alternatively, the influence of CA may not be accurately described in our model. Thus, even though the sensitivity tests with the present ExClump38 model predicts otherwise, our experimental data showing no CA influence on the magnitude of the dip are actually robust. Along this line, it is noteworthy that the reaction mechanisms of uncatalyzed versus CA-mediated CO<sub>2</sub> hydration to HCO<sub>3</sub> appear fundamentally different. In the CA-mediated case, a H<sub>2</sub>O molecule is rapidly deprotonated at the enzyme's zinc-containing active site, which releases H<sup>+</sup> while OH<sup>-</sup> is retained on the enzyme as a Zn-OH<sup>-</sup> unit. This then binds and reacts with CO<sub>2</sub> to generate HCO<sub>3</sub> (Paneth and O'Leary, 1985; Silverman and Lindskog, 1988; Guo et al., 2011):

$$E \cdot \text{ZnH}_2\text{O} \leftrightarrow E \cdot \text{ZnOH}^- + \text{H}^+$$
 (30)

and

$$E \cdot \text{ZnOH}^- + \text{CO}_2 \leftrightarrow E \cdot \text{Zn(OH}^-) \text{CO}_2$$
  
 
$$\leftrightarrow E \cdot \text{ZnHCO}_3^- \leftrightarrow E \cdot \text{ZnH}_2 \text{O} + \text{HCO}_3^-$$
(31)

where E signifies CA enzyme. This sequence shows that, although the end result is hydration of CO<sub>2</sub> (Eq. (3)), what happens to CO2 itself is actually more akin to hydroxylation. So,  ${}^{13}\alpha_{k_{+1}}^{KIF}$  may not be the correct parameter to be tuned for the effect of CA. Lastly, as previously noted in Zeebe (2014) and Yumol et al. (2020), there appears to be some caveats regarding the work of O'Leary and colleagues. First, the kinetic fractionation of 1.0069 (or ~6.9‰) for conversion of  $CO_{2(g)}$  to  $HCO_3^-$  via the hydration pathway by Marlier and O'Leary (1984) is anomalously small amongst the values established in other studies (see Table 1 in Yumol et al. (2020)). Moreover, their work is oddly cited in a subsequent study by the same group (O'Leary et al., 1992) with a value of 13%, not 6.9%, without any explanation. Then, from the value of  $^{13}\alpha^{EQ}_{HCO_2^--CO2(g)}$  by Zhang et al. (1995), this requires the kinetic fractionation for the reverse reaction to be revised to ~22% from the original value of 14.7% reported in Marlier and O'Leary (1984) on the basis of degassing experiments. Since Paneth and O'Leary (1985) employed the same degassing experiments for CA, their data should be taken with caution.

# 4.4.3. ExClump38 simulations for various scenarios

Disequilibrium in DCP in terms of both  $\delta^{18}O$  and  $\Delta_{47}$  can be propagated to carbonate minerals when mineral formation greatly outpaces isotopic equilibration in DCP (Tripati et al., 2015; Watkins and Hunt, 2015; Guo et al., 2019; Guo, 2020), thereby critically biasing paleotemperature reconstructions. Provided with good model-data agreement (Fig. 9), we can use the ExClump38 model to test

various physicochemical scenarios for the timescale and trajectory of isotopic equilibration in DCP.

The modeled TS2 equilibration path may be compared to a set of hypothetical paths to the same equilibrium, but from different initial states (Fig. 10). Path-1 and Path-2 in Fig. 10 have the same initial  $\delta^{18}O_{DCP}$  as our TS2 experiments, but their starting  $\Delta_{47}$  is exactly at or above equilibrium. Even under these circumstances, analogous to TS2 path,  $\Delta_{47}$  of DCP initially drops below equilibrium during the early part of equilibration. In contrast, if equilibration starts from the same  $\Delta_{47}$  as TS2 but  $\delta^{18}O_{DCP}$  above equilibrium (Path-3), there is a  $\Delta_{47}$  overshoot during equilibration. This is inevitable because, as described in Section 2.3.1, [2866] decreases more rapidly than [3866] during the early part of isotopic equilibration in DCP. Path-4 shows a unique case where DCP is already in  $\delta^{18}$ O equilibrium but out of  $\Delta_{47}$  equilibrium. In this case,  $\Delta_{47}$  equilibration no longer follows nonfirst-order kinetics because equilibration only involves changes in <sup>13</sup>C-<sup>18</sup>O clumps in DCP having a fixed <sup>18</sup>O inventory. As Eq. (14) implies, this process follows a first-order exponential decay function. For all of these scenarios, the timescale for isotopic equilibration is identical.

We also examine the effect of solution pH using the ExClump38 model (Fig. 10cd), which should be of particular relevance to, for example, coral calcification and speleothem formation that involves alterations in solution pH (Al-Horani et al., 2003; Daëron et al., 2011). As is the case for  $\delta^{18}$ O (and as shown previously in UZ12),  $\Delta_{47}$  equilibration takes longer at higher pH due to a decline in [CO<sub>2</sub> (aq), only through which formations or break-ups of  $^{6}$ C- $^{18}$ O bonds are possible. In addition,  $\delta^{18}$ O and  $\Delta_{47}$  of DCP at which the respective equilibration trajectory plateaus change systematically with pH. This is due to the pH-induced shifts in the relative abundance of HCO<sub>3</sub> and  $CO_3^{2-}$  in DCP, each having distinct equilibrium  $\delta^{18}O$  and  $\Delta_{47}$  signatures (Fig. 1, Beck et al., 2005; Uchikawa and Zeebe, 2013; Tripati et al., 2015). In our simulations, however, the magnitude of excess  $\Delta_{47}$  disequilibrium (i.e., the dip) remains almost constant in all cases (Fig. 10d).

For the evaluation of temperature effects shown in Fig. 10ef, two adjustments were made in the ExClump38 model. In the default set-up, equilibrium  $\delta^{18}$ O and  $\Delta_{47}$  signatures of the  $HCO_3^-$  and  $CO_3^{2-}$  are based on the experimental constraints by Uchikawa and Zeebe (2013) and Tripati et al. (2015), which are only valid at 25 °C. For defining equilibrium  $\delta^{18}$ O of HCO<sub>3</sub> and CO<sub>3</sub> beyond 25 °C, we used the temperature-dependence of  ${}^{18}\alpha^{EQ}_{\text{HCO}_3^--\text{H}_2\text{O}}$  and  ${}^{18}\alpha^{EQ}_{\text{CO}_3^2^--\text{H}_2\text{O}}$ by Beck et al. (2005). Although we are unaware of direct experimental constraints for equilibrium  $\Delta_{47}$  of the respective DIC species beyond 25 °C, ab-initio calculations by Hill et al. (2020) show temperature controls on the degree of <sup>13</sup>C-<sup>18</sup>O clumping in HCO<sub>3</sub> and CO<sub>3</sub><sup>2-</sup>. For this exercise, we derived the temperature-sensitivity of the equilibrium  $\Delta_{47}$ of HCO<sub>3</sub> and CO<sub>3</sub><sup>2</sup> by applying polynomial fit to a set of Hill et al. (2020) calculations between 0 and 100 °C, after accounting for offsets from the direct experimental constraints by Tripati et al. (2015) (see Table A3 and Fig. A1 in the detailed model description in Supplementary Materials).

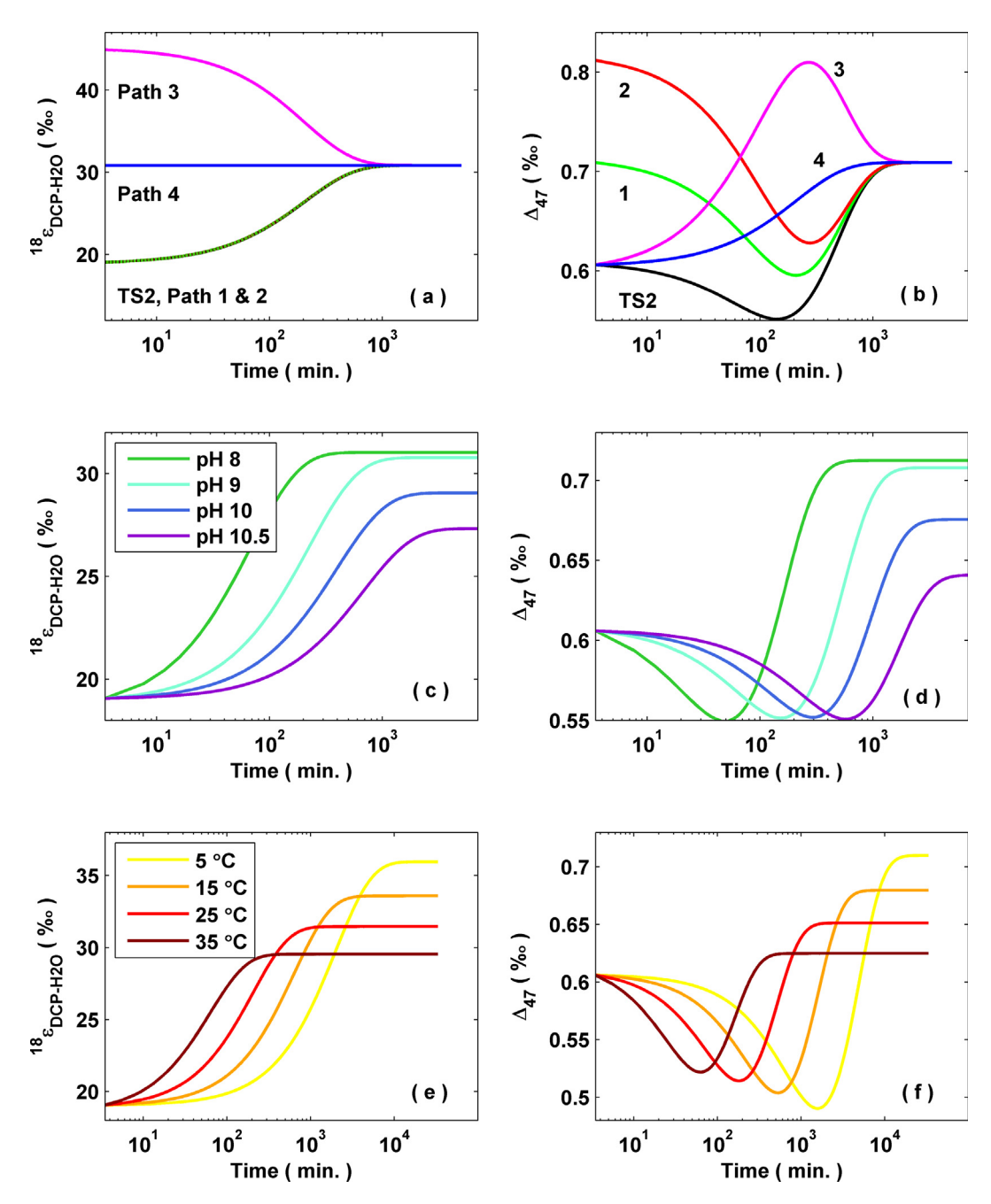


Fig. 10. Case studies of isotopic equilibration under various scenarios by the ExClump38 model. (a and b) Comparison of the TS2 equilibration path to hypothetical paths toward the common equilibrium but from different starting points. Equilibration in DCP for Path 1 and 2 starts from the  $\delta^{18}$ O same as TS2 but at  $\Delta_{47}$  exactly at or higher than equilibrium (Path 1 and Path 2, respectively). Path 3 starts from the same  $\Delta_{47}$  as TS2 but  $\delta^{18}$ O higher than equilibrium. Path 4 starts from the same  $\Delta_{47}$  disequilibrium as TS2 but  $\delta^{18}$ O exactly at equilibrium. (c and d) Effect of solution pH on the timescale and trajectory of isotopic equilibration. (e and f) Effect of temperature on isotopic equilibration. The baseline modeling conditions are kept the same as TS2 for the simulations of pH and temperature effects.

Chemical reaction and isotope exchange rates normally increases with temperature. An increase in temperature hence leads to more rapid isotopic equilibration in DCP for both  $\delta^{18}O$  and  $\Delta_{47}$  (Fig. 10ef). Our simulations also indicate a systematic decrease in the  $\delta^{18}O$  and  $\Delta_{47}$  equilibrium at higher temperature. This is consistent with Beck et al. (2005) and SS18. Note that the  $\Delta_{47}$  dips are slightly shallower at higher temperatures (Fig. 10f). This is some-

what counter-intuitive, as  $^{13}\alpha_{k_{+1}}^{KIF}$  and  $^{13}\alpha_{k_{+4}}^{KIF}$  that play central roles in determining the magnitude of the dip (see Section 4.4.1 and Fig. S5) are assumed to be independent of temperature and constant in the ExClump38 model, following the outcomes of previous studies (Clark and Lauriol, 1992; Yumol et al., 2020; Yumol et al., 2020; Guo, 2020; Christensen et al., 2021). Yet,  $^{13}\alpha_{k_{+1}}^{KIF}$  and  $^{13}\alpha_{k_{+4}}^{KIF}$  are combined with other constants (K's, K's and  $\alpha^{EQ}$ 's) to derive

the forward and backward rate constants for Eq. (19) and Eq. (20) ( $^{13}k_{\pm 1}$  and  $^{13}k_{\pm 4}$ ) for the differential equations solved by the ExClump38 model (see the full model description in Supplementary Materials). As those are all temperature-dependent,  $^{13}k_{\pm 1}$  and  $^{13}k_{\pm 4}$  must vary with temperature, despite  $^{13}\alpha_{k_{+1}}^{KIF}$  and  $^{13}\alpha_{k_{+4}}^{KIF}$  being a single value.

Is the temperature effect predicted by the ExClump38 model (Fig. 10f) consistent with available experimental data? SS18 ran their experiments at 5, 15 and 25 °C. Yet, their data show fairly similar magnitude of the  $\Delta_{47}$  dip at all temperatures (roughly -0.05 to -0.06%, see their Fig. 2B). But an important remark is that the shoaling of the excess  $\Delta_{47}$  disequilibrium predicted by the ExClump38 model is only ~0.02‰ per 10 °C of temperature increase (Fig. 10f), which is smaller than the uncertainties for some of the  $\Delta_{47}$  data in SS18 (also see Section 4.3.1. for other caveats in their experimental data). Weise and Kluge (2020) similarly studied the isotopic equilibration kinetics between 40 and 90 °C. In all of their experimental series. however, they found no clear evidence of non-first-order kinetics for  $\Delta_{47}$  equilibration and concluded that both  $\delta^{18}O$  and  $\Delta_{47}$  equilibration follow first-order exponential decay. Weise and Kluge (2020) further argued that the non-first-order characteristic in  $\Delta_{47}$  equilibration demonstrated in SS18 is likely an artifact due to the temporal drift in  $\delta^{13}$ C of DCP with time in their experimental results (Fig. S1a). This point was also raised in a recent experimental study by Thaler et al. (2020). However, we find this argument to be invalid because  $\Delta_{47}$  equilibration clearly followed non-first-order kinetics in our experimental data that apparently show no drift in  $\delta^{13}$ C of DCP (Fig. 3 and Fig. 4). We instead argue that the reason why Weise and Kluge (2020) did not find clear non-first-order features is the narrow range of  $\delta^{18}$ O changes in DCP in their experiments (~4% at most, as opposed to easily over 10% in SS18 and our experiments). This resembles the situation shown by Path-4 in Fig. 10ab, where the  $\Delta_{47}$  equilibration kinetics becomes first-order. If  $\delta^{18}O$  of DCP during equilibration varied over a much wider range, the ExClump38 model predicts the non-first-order characteristics to be expressed in the experimental condition of Weise and Kluge (2020) (Fig. S6). And, because their  $\delta^{18}$ O of DCP is initially higher than equilibrium, the non-first-order kinetics should result in an overshoot (e.g., Path-3 in Fig. 10ab), rather than a dip in the  $\Delta_{47}$  equilibration trajectory (this study, SS18). Yet, successfully capturing such a signal can be difficult in their case due to high experimental temperatures, at which isotopic equilibration in DCP should be very rapid. In any case, more experimental work is needed to verify the model-predicted temperature effect on the degree of excess  $\Delta_{47}$  disequilibrium. And, success of such experiments hinges on substantially reducing the uncertainty and noise in  $\Delta_{47}$  data.

#### 4.5. Implications

For this study, we developed the ExClump38 model that can successfully replicate the trajectory and time-course of  $\delta^{18}$ O and  $\Delta_{47}$  equilibration in DCP under both normal and CA-catalyzed conditions revealed by experimental data from independent studies (this study, SS18, Weise and Kluge, 2020). This model can be a particularly useful tool for the planning of laboratory experiments in which full isotopic equilibrium in DCP with H<sub>2</sub>O is absolutely critical (e.g., calibrations of the paleothermometers based on laboratory-grown inorganic carbonates). And, for that, our experimental work clearly shows that commercially readily accessible bovine CA is highly effective in promoting isotopic equilibrium in the dissolved carbonate system (e.g., Watkins et al., 2013; Watkins et al., 2014; Tripati et al., 2015; Kelson et al., 2017; Thaler et al., 2020).

Our simulations by the ExClump38 model show that disequilibrium in both  $\delta^{18}$ O and  $\Delta_{47}$  is more persistent (and potentially more extensive) in colder and more alkaline DCP (Fig. 10), which is particularly relevant to the isotopic state of the extracellular calcifying fluid (ECF) of cold-water and deep-sea corals for example. However, as demonstrated by the results from our experiments with CA enzyme,  $\Delta_{47}$  disequilibrium in ECF (for potential drivers, see Thiagarajan et al., 2011; Spooner et al., 2016) can be relieved by CA. Given that a wide range of marine calcareous organisms possess CA and it apparently plays some roles in biological calcification (Moya et al., 2008; de Goeyse et al., 2021; Zhang et al., 2021), CA should be an important consideration when discussing  $\Delta_{47}$  vital effects in general. As the final remark, we note that the ExClump38 model can be expanded from the current version (exclusively designed for closed systems) for applications to such biological or other open systems by reimplementing the flux terms originally considered in Chen et al. (2018) or Christensen et al. (2021) in future studies.

## 5. CONCLUSIONS

In this study, we investigated the timescales and trajectories of  $\delta^{18}$ O and  $\Delta_{47}$  equilibration in the dissolved carbonate pool (DCP, which is the sum of  $[HCO_3^-]$  and  $[CO_3^{2-}]$ ) based on time-series BaCO<sub>3</sub> samples of UZ12 that were quantitatively precipitated from NaHCO<sub>3</sub> solutions undergoing isotopic equilibration. Importantly, we additionally analyzed samples precipitated from the NaHCO<sub>3</sub> solutions supplemented with carbonic anhydrase (CA), an enzyme possessed by many marine calcareous organisms and known to accelerate isotopic exchange between DCP and H<sub>2</sub>O via its catalysis of CO2 hydration. Our data show that, while the timescales for equilibration are broadly similar for  $\delta^{18}$ O and  $\Delta_{47}$ , the paths toward equilibrium are fundamentally different. As previously shown in UZ12,  $\delta^{18}$ O equilibration in DCP follows an asymptotic path toward equilibrium that can be modeled by a first-order exponential decay function. However,  $\Delta_{47}$  equilibration initially departs to even stronger disequilibrium and subsequently turns its course toward equilibrium, resulting in an apparent non-first-order kinetics (a pattern consistent with SS18). Sensitivity analyses with our ExClump38

model point to kinetic carbon isotope fractionation associated with CO<sub>2</sub> hydration and hydroxylation as the underlying drivers of the dip in the  $\Delta_{47}$  equilibration trajectory. In the presence of CA, there is a clear reduction in the time needed for  $\delta^{18}O$  and  $\Delta_{47}$  equilibrium in DCP with an increase in enzyme concentration. Yet, the nonfirst-order feature for the  $\Delta_{47}$  equilibration trajectory is still present and the extent of excess  $\Delta_{47}$  disequilibrium remains fairly constant at all concentrations examined here. In other words, within the concentration range tested here, our data suggest that CA only shortens the timescales of  $\delta^{18}$ O and  $\Delta_{47}$  equilibration, without altering the overall patterns of their equilibration trajectories. Our simulations with the ExClump38 model predict more pronounced and prolonged  $\Delta_{47}$  disequilibrium for colder and more alkaline environments, as expected for the site of calcification in cold-water and/or deep-sea corals for instance. However, our experimental results demonstrate that  $\Delta_{47}$  disequilibrium can be alleviated by the presence of CA.

# **Declaration of Competing Interest**

The authors declare that they have no known competing financial interests or personal relationships that could have appeared to influence the work reported in this paper.

#### ACKNOWLEDGEMENTS

Nami Kitchen, Uri Ryb, Fuyun Cong and Yuchen Liu are thanked for their help in the lab. We credit the original work of Staudigel and Swart (2018) that inspired us to launch this study. We are grateful to Jim Watkins, Philip Staudigel and an anonymous reviewer for their technical reviews and follow-up discussions with us, which were instrumental in improving this paper. This study was supported by U.S. NSF grants OCE1558699 and OCE2048436 to REZ and JU. SC received financial support from the China Scholarship Council. SOEST Pub. #11384.

# APPENDIX A. SUPPLEMENTARY DATA

Supplementary data to this article can be found online at https://doi.org/10.1016/j.gca.2021.08.014. The Matlab codes for the ExClump38 model can be freely downloaded from the EarthChem Library data repository system (https://doi.org/10.26022/IEDA/112078).

#### REFERENCES

- Adkins J. F., Boyle E. A., Curry W. B. and Lutringer A. (2003) Stable isotopes in deep-sea corals and a new mechanism for 'vital effects'. *Geochim. Cosmochim. Acta* 67, 1129–1143.
- Affek H. P. (2013) Clumped isotope equilibrium and the rate of isotope exchange between CO<sub>2</sub> and water. *Am. J. Sci.* **313**, 309–325.
- Affek H. P. and Zaarur S. (2012) Kinetic isotope effect in CO<sub>2</sub> degassing: Insight from clumped and oxygen isotopes in laboratory precipitation experiments. *Geochim. Cosmochim. Acta* 143, 319–330.
- Al-Horani F. A., Al-Moghrabi S. M. and de Beer D. (2003) Microsensor study of photosynthesis and calcification in the

- scleractinian coral, *Galaxea fascicularis*: Active internal carbon cycle. *J. Exp. Mar. Biol. Ecol.* **288**, 1–15.
- Bajnai D., Guo W., Spötl C., Coplen T. B., Methner K., Löffler N., Krsnik E., Gischler E., Hensen M., Henkel D., Price G. D., Raddatz J., Scholz D. and Fiebig J. (2020) Dual clumped isotope thermometry resolves kinetic biases in carbonate formation temperatures. *Nat. Commun.* 11, 4005.
- Beck W. C., Grossman E. L. and Morse J. W. (2005) Experimental studies of oxygen isotope fractionation in the carbonic acid system at 15° 25° and 40°C. *Geochim. Cosmochim. Acta* **69**, 3493–3503.
- Bertucci A., Tambutté S., Supuran C. T., Allemand D. and Zoccola D. (2011) A new coral carbonic anhydrase in *Stylophora pistillata. Mar. Biotechnol.* 13, 992–1002.
- Boettger J. D. and Kubicki J. D. (2021) Equilibrium and kinetic isotopic fractionation in the CO<sub>2</sub> hydration and hydroxylation reactions: Analysis of the role of hydrogen-bonding via quantum mechanical calculations. *Geochim. Cosmochim. Acta* 292, 37–63.
- Bonifacie M., Calmels D., Eiler J. M., Horita J., Chaduteau C., Vasconcelos C., Agrinier A., Katz A., Passey B. H., Ferry J. M. and Bourrand J.-J. (2017) Calibration of the dolomite clumped isotope thermometer from 25 to 350 °C, and implications for a universal calibration for all (Ca, Mg, Fe)CO<sub>3</sub> carbonates. *Geochim. Cosmochim. Acta* 200, 255–279.
- Böttcher M. E. (1996) <sup>18</sup>O/<sup>16</sup>O and <sup>13</sup>C/<sup>12</sup>C fractionation during the reaction of carbonates with phosphoric acid: effects of cationic substitution and reaction temperature. *Isotopes Environ. Health Stud.* **32**, 299–305.
- Brand W. A., Assonov S. S. and Coplen T. B. (2010) Correction for the <sup>17</sup>O interference in δ(<sup>13</sup>C) measurements when analyzing CO<sub>2</sub> with stable isotope mass spectrometry (IUPAC Technical Report). *Pure Appl. Chem.* 82, 1719–1733.
- Chen S., Gagnon A. C. and Adkins J. F. (2018) Carbonic anhydrase, coral calcification and a new model of stable isotope vital effects. *Geochim. Cosmochim. Acta* 236, 179–197.
- Chen S., Ryb U., Piasecki A. M., Lloyd M. K., Baker M. B. and Eiler J. M. (2019) Mechanism of solid-state clumped isotope reordering in carbonate minerals from aragonite heating experiments. *Geochim. Cosmochim. Acta* 258, 156–173.
- Christensen J. N., Watkins J. M., Devriendt L. S., DePaolo D. J., Conrad M. E., Voltolini M., Yang W. and Dong W. (2021) Isotopic fractionation accompanying CO<sub>2</sub> hydroxylation and carbonate precipitation from high pH waters at the Cedars, California, USA. *Geochim. Cosmochim. Acta* 301, 91–115.
- Clark I. D. and Lauriol B. (1992) Kinetic enrichment of stable isotopes in cryogenic calcites. Chem. Geol. 102, 217–228.
- Clark I. D., Fontes J. C. and Fritz P. (1992) Stable isotope disequilibria in travertine from high pH waters: laboratory investigations and field observations from Oman. *Geochim. Cosmochim. Acta* 56, 2041–2050.
- Clog M., Stolper D. and Eiler J. M. (2015) Kinetics of  $CO_{2(g)}$ - $H_2O_{(1)}$  isotope exchange, including mass 47 isotopologues. *Chem. Geol.* **395**, 1–10.
- Coplen T. B., Kendall C. and Hopple J. (1983) Comparison of stable isotope reference samples. *Nature* 302, 236–238.
- Coplen T. B. (2007) Calibration of the calcite-water oxygen-isotope geothermometer at Devils Hole, Nevada, a natural laboratory. *Geochim. Cosmochim. Acta* 71, 3948–3957.
- Daëron M., Guo W., Eiler J. M., Genty D., Blamart D., Boch R.,
   Drysdale R., Maire R., Wainer K. and Zanchetta G. (2011)
   <sup>13</sup>C<sup>18</sup>O clumping in speleothems: Observations from natural caves and precipitation experiments. *Geochim. Cosmochim. Acta* 75, 3303–3317.

- Daëron M., Balamart D., Peral M. and Affek H. P. (2016) Absolute isotopic abundance ratios and the accuracy of Δ<sub>47</sub> measurements. Chem. Geol. 442, 83–96.
- Daëron M., Drysdale R. N., Peral M., Huyghe D., Blamart D., Colpen T. B., Lartaud F. and Zanchetta G. (2019) Most Earthsurface calcite precipitate out of isotopic equilibrium. *Nat. Commun.* 10, 429.
- de Goeyse S., Webb A. E., Reichart G.-J. and de Nooijer L. J. (2021) Carbonic anhydrase is involved in calcification by the benthic foraminiferal *Amphistegina lessonii*. *Biogeosciences* 18, 393–401.
- Dennis K. J. and Schrag D. P. (2010) Clumped isotope thermometry of carbonatites as an indicator of diagenetic alteration. *Geochim. Cosmochim. Acta* 74, 4110–4122.
- Dennis K. J., Affek H. P., Passey B. H., Schrag D. P. and Eiler J. M. (2011) Defining an absolute reference frame for 'clumped' isotope studies of CO<sub>2</sub>. *Geochim. Cosmochim. Acta* 75, 7117–7131.
- Devriendt L. S., Watkins J. M. and McGregor H. V. (2017) Oxygen isotope fractionation in the CaCO<sub>3</sub>-DIC-H<sub>2</sub>O system. *Geochim. Cosmochim. Acta* 214, 115–142.
- Dietzel M., Tang J., Leis A. and Köhler S. J. (2009) Oxygen isotope fractionation during inorganic calcite precipitation Effects of temperature, precipitation rate and pH. *Chem. Geol.* **268**, 107–115
- Eagle R. A., Eiler J. M., Tripati A. K., Ries J. B., Freitas P. S., Hiebenthal C., Wanamaker, Jr., A. D., Taviani M., Elliot M., Marenssi S., Nakamura K., Ramirez P. and Roy K. (2013) The influence of temperature and seawater carbonate saturation state on <sup>13</sup>C–<sup>18</sup>O bond ordering in bivalve mollusks. *Biogeo-sciences* 10, 4591–4606.
- Eiler J. M. (2007) "Clumped-isotope" geochemistry the study of naturally-occuring, multiply-substituted isotopologues. *Earth. Planet. Sci. Lett.* 262, 309–327.
- Eiler J. M. (2011) Paleoclimate reconstruction using carbonate clumped isotope thermometry. *Quat. Sci. Rev.* **30**, 3575–3588.
- Falk E. S., Guo W., Paukert A. N., Matter J. M., Mervine E. M. and Kelemen P. B. (2016) Controls on the stable isotope compositions of travertine from hypersaline springs in Oman: Insights from clumped isotope measurements. *Geochim. Cosmochim. Acta* 192, 1–28.
- Ghosh P., Adkins J., Affek H., Balta B., Guo W., Schauble E. A., Schrag D. and Eiler J. M. (2006) <sup>13</sup>C-<sup>18</sup>O bonds in carbonate minerals: A new kind of paleothermometer. *Geochim. Cos-mochim. Acta* 70, 1439–1456.
- Guo D., Thee H., da Silva G., Chen J., Fei W., Kentish S. and Stevens G. W. (2011) Borate-catalyzed carbon dioxide hydration via the carbonic anhydrase mechanism. *Environ. Sci. Technol.* 45, 4802–4807.
- Guo W. (2009) Carbonate clumped isotope thermometry: application to carbonaceous chondrites and effects of kinetic isotope fractionation PhD thesis. California Institute of Technology.
- Guo W. (2020) Kinetic clumped isotope fractionation in the DIC-H<sub>2</sub>O-CO<sub>2</sub> system: Patterns, controls, and implications. *Geochim. Cosmochim. Acta* 268, 230–257.
- Guo W., Mosenfelder J. L., Goddard, III, W. A. and Eiler J. M. (2009) Isotopic fractions associated with phosphoric acid digestion of carbonate minerals: Insights from first-principles theoretical modeling and clumped isotope measurements. *Geochim. Cosmochim. Acta* 73, 7203–7225.
- Guo W. and Zhou C. (2019) Patterns and controls of disequilibrium isotope effects in speleothems: Insights from an isotope-enabled diffusion-reaction model and implications for quantitative thermometry. *Geochim. Cosmochim. Acta* 267, 196–226.
- Guo Y., Deng W. and Wei G. (2019) Kinetic effects during the experimental transition of aragonite to calcite in aqueous

- solution: Insights from clumped and oxygen isotope signatures. *Geochim. Cosmochim. Acta* **248**, 210–230.
- Harned H. S. and Davis R. J. (1943) The ionization constant of carbonic acid in water and the solubility of carbon dioxide in water and aqueous salt solutions from 0 to 50 °C. *J. Am. Chem. Soc.* **65**, 2030–2037.
- Harned H. S. and Owen B. B. (1958) *The Physical Chemistry of Electrolytic Solutions*. Reinhold, New York.
- Harned H. S. and Scholes S. R. J. (1941) The ionization constant of HCO<sub>3</sub><sup>-</sup> from 0 to 50 °C. *J. Am. Chem. Soc.* **63**, 1706–1709.
- Henkes G. A., Passery B. H., Wanamaker, Jr., A. D., Grossman E. L., Ambrose, Jr., W. G. and Carroll M. L. (2013) Carbonate clumped isotope compositions of modern marine mollusk and brachiopod shells. *Geochim. Cosmochim. Acta* 106, 307–325.
- Hill P. S., Schauble E. A. and Tripati A. K. (2020) Theoretical constraints on the effects of added cations on clumped, oxygen, and carbon isotope signatures of dissolved inorganic carbon species and minerals. *Geochim. Cosmochim. Acta* 269, 496–539.
- Kelson J. R., Huntington K. W., Schauer A. J., Saenger C. and Lechler A. R. (2017) Toward a universal carbonate clumped isotope calibration: Diverse synthesis and preparatory methods suggest a single temperature relationship. *Geochim. Cosmochim.* Acta 197, 104–131.
- Kim S.-T. and O'Neil J. R. (1997) Equilibrium and nonequilibrium oxygen isotope effects in synthetic carbonates. *Geochim. Cosmochim. Acta* **61**, 3461–3475.
- Kim S.-T., O'Neil J. R., Hillaire-Marcel C. and Mucci A. (2007) Oxygen isotope fractionation between synthetic aragonite and water: Influence of temperature and Mg<sup>2+</sup> concentration. *Geochim. Cosmochim. Acta* 71, 4704–4715.
- Kluge T., Affek H. P., Zhang Y. G., Dublyansky Y., Spötl C., Immenhauser A. and Richter D. K. (2014) Clumped isotope thermometry of cryogenic cave carbonates. *Geochim. Cos-mochim. Acta* 126, 541–554.
- Kluge T., John C. M., Jourdan A.-L., Davis S. and Crawshaw J. (2015) Laboratory calibration of the calcium carbonate clumped isotope thermometer in the 25–250 °C temperature range. *Geochim. Cosmochim. Acta* 157, 213–227.
- Levitt N. P., Eiler J. M., Romanek C. S., Beard B. L., Xu H. and Johnson C. M. (2018) Near equilibrium <sup>13</sup>C-<sup>18</sup>O bonding during inorganic calcite precipitation under chemo-stat conditions. *Geochem. Geophys. Geosyst.* 19, 901–920.
- Lloyd M. K., Ryb U. and Eiler J. M. (2019) Experimental calibration of clumped isotope reordering in dolomite. Geochim. Cosmochim. Acta 242, 1–20.
- Marlier J. F. and O'Leary M. H. (1984) Carbon kinetic isotope effects on the hydration of carbon dioxide and the dehydration of bicarbonate ion. *J. Am. Chem. Soc.* **106**, 5054–5057.
- McConnaughey T. A. (1989) <sup>13</sup>C and <sup>18</sup>O isotopic disequilibrium in biological carbonates: I. *Patterns. Geochim. Cosmochim. Acta* **53**, 151–162.
- McCrea J. M. (1950) On the isotopic chemistry of carbonates and a paleotemperature scale. *J. Chem. Phys.* **18**, 849–857.
- Mills G. A. and Urey H. C. (1940) The kinetics of isotopic exchange between carbon dioxide, bicarbonate ion, carbonate ion and water. *J. Am. Chem. Soc.* **62**, 1019–1026.
- Mook W. G. (1986) <sup>13</sup>C in atmospheric CO<sub>2</sub>. *Neth. J. Sea Res.* **20** (2/3), 211–223.
- Morley S. K., Brito T. V. and Welling D. T. (2018) Measures of model performance based on the log accuracy ratio. Space Weather 16, 69–88.
- Moya A., Tambutté S., Bertucci A., Tambutté E., Lotto S., Vullo D., Supuran C. T., Allemand D. and Zoccola D. (2008) Carbonic anhydrase in the Scleractinian coral *Stylophora pistillata*: Characterization, localization, and role in biomineralization. *J. Biol. Chem.* 283, 25475–25484.

- O'Leary M. H., Madhaven S. and Paneth P. (1992) Physical and chemical basis of carbon isotope fractionation in plants. *Plant, Cell Environ.* **15**, 1099–1104.
- Paneth P. and O'Leary M. H. (1985) Carbon isotope effect on dehydration of bicarbonate ion catalyzed by carbonic anhydrase. *Biogeochemistry* **24**, 5143–5147.
- Pinsent B. R. W., Pearson L. and Rooughton F. J. W. (1956) The kinetics of combination of carbon dioxide with hydroxide ions. *Trans. Taraday Soc.* 52, 2930–2934.
- Riechelmann D. F. C., Deininger M., Scholz D., Riechelmann S., Schröder-Ritzrau A., Spötl C., Richter D. K., Mangini A. and Immenhauser A. (2013) Disequilibrium carbon and oxygen isotope fractionation in recent cave calcite: Comparison of cave precipitates and model data. *Geochim. Cosmochim. Acta* 103, 232–244.
- Saenger C., Affek H. P., Felis T., Thiagarajan N., Lough J. M. and Holcomb M. (2012) Carbonate clumped isotope variability in shallow water corals: Temperature dependence and growthrelated vital effects. *Geochim. Cosmochim. Acta* 99, 224–242.
- Schauble E. A., Ghosh P. and Eiler J. M. (2006) Preferential formation of <sup>13</sup>C<sup>-18</sup>O bonds in carbonate minerals, estimated using first-principles lattice dynamics. *Geochim. Cosmochim. Acta* **70**, 2510–2529.
- Schauer A. J., Kelson J., Saenger C. and Huntington K. W. (2016) Choice of  $^{17}$ O correction affects clumped isotope ( $\Delta_{47}$ ) values of CO<sub>2</sub> measured with mass spectrometry. *Rapid Commun. Mass Spectrom.* **30**, 2607–2616.
- Silverman D. N. and Lindskog S. (1988) The catalytic mechanism of carbonic anhydrase: Implications of a rate-limiting protolysis of water. *Acc. Chem. Res.* **21**, 30–36.
- Spero H. J., Bijma J., Lea D. W. and Bemis B. E. (1997) Effect of seawater carbonate concentration on foraminiferal carbon and oxygen isotopes. *Nature* 390, 497–500.
- Spooner P. T., Guo W., Robinson L. F., Thiagarajan N., Hendry K. R., Rosenheim B. E. and Leng M. J. (2016) Clumped isotope composition of cold-water corals: A role for vital effects? Geochim. Cosmochim. Acta 179, 123–141.
- Staudigel P. T. and Swart P. K. (2018) A kinetic difference between <sup>12</sup>C- and <sup>13</sup>C-bound oxygen exchange rates results in decoupled δ<sup>18</sup>O and Δ<sub>47</sub> values of equilibrating DIC solutions. *Geochem. Geophys. Geosyst.* **19**. doi.10.1029/2018GC007500.
- Tambutté S., Tambutté E., Zoccola D., Caminiti N., Lotto S., Moya S., Allemand D. and Adkins J. F. (2007) Characterization and role of carbonic anhydrase in the calcification process of the axoozanthellate coral *Tubastrea aurea*. *Mar. Biol.* **151**, 71–83
- Tang J., Dietzel M., Fernandez A., Tripati A. K. and Rosenheim B. E. (2014) Evaluation of kinetic effects on clumped isotope fractionation (Δ<sub>47</sub>) during inorganic calcite precipitation. *Geochim. Cosmochim. Acta* 134, 120–136.
- Thaler C., Katz A., Bonifacie M., Ménez B. and Ader M. (2020) Oxygen isotope composition of waters recorded in carbonates in strong clumped and oxygen isotopic disequilibrium. *Biogeo-sciences* 17, 1731–1744.
- Thiagarajan N., Adkins J. F. and Eiler J. M. (2011) Carbonate clumoed isotope thermometry of deep-sea corals and implications for vital effects. *Geochim. Cosmochim. Acta* 75, 4416–4425.
- Tripati A. K., Hill P. S., Eagle R. A., Mosenfelder J. L., Tang J.,
  Schauble E. A., Eiler J. M., Zeebe R. E., Uchikawa J., Coplen T. B., Ries J. B. and Henry D. (2015) Beyond temperature:
  Clumped isotope signatures in dissolved inorganic carbon species and the influence of solution chemistry on carbonate mineral composition. *Geochim. Cosmochim. Acta* 166, 344–371.

- Uchikawa J. and Zeebe R. E. (2012) The effect of carbonic anhydrase on the kinetics and equilibrium of oxygen isotope exchange in the  $CO_2$ - $H_2O$  system: Implications for  $\delta^{18}O$  vital effects in biogenic carbonates. *Geochim. Cosmochim. Acta* **95**, 15–34.
- Uchikawa J. and Zeebe R. E. (2013) No discernable effect of Mg<sup>2+</sup> ions on the equilibrium oxygen isotope fractionation in the CO<sub>2</sub>-H<sub>2</sub>O system. *Chem. Geol.* **343**, 1–11.
- Usdowski E., Michaelis J., Böttcher M. E. and Hoefs J. (1991) Factors for the oxygen isotope equilibrium fractionation between aqueous and gaseous CO<sub>2</sub>, carbonic acid, bicarbonate, carbonate, and water (19 °C). *Z. Phys. Chem. A* **114**, 1734–1740.
- Urey H. (1947) The thermodynamic properties of isotopic substances. J. Chem. Soc. (Resumed), 562–581.
- Watkins J. M., Nielsen L. C., Ryerson F. J. and DePaolo D. J. (2013) The influence of kinetics on the oxygen isotope composition of calcium carbonate. *Earth Planet. Sci. Lett.* 375, 349–360
- Watkins J. M., Hunt J. D., Ryerson F. J. and DePaolo D. J. (2014) The influence of temperature, pH, and growth rate on the  $\delta^{18}$ O composition of inorganically precipitated calcite. *Earth Planet. Sci. Lett.* **404**, 332–343.
- Watkins J. M. and Hunt J. D. (2015) A process-based model for non-equilibrium clumped isotope effects in carbonates. *Earth Planet. Sci. Lett.* 432, 152–165.
- Weise A. and Kluge T. (2020) Isotope exchange rates in dissolved inorganic carbon between 40 °C and 90 °C. *Geochim. Cosmochim. Acta* **268**, 56–72.
- Yumol L. M., Uchikawa J. and Zeebe R. E. (2020) Kinetic isotope effects during CO<sub>2</sub> hydration: Experimental results for carbon and oxygen fractionation. *Geochim. Cosmochim. Acta* 279, 189– 203
- Zaarur S., Affek H. P. and Brandon M. T. (2013) A revised calibration of the clumped isotope thermometer. *Earth Planet Sci. Lett.* 382, 47–57.
- Zeebe R. E. (2007) An expression for the overall oxygen isotope fractionation between the sum of dissolved inorganic carbon and water. *Geochem. Geophys. Geosyst.* **8**, Q09002.
- Zeebe R. E. (2014) Kinetic fractionation of carbon and oxygen isotopes during hydration of carbon dioxide. *Geochim. Cosmochim. Acta* **139**, 540–552.
- Zeebe R. E. (2020) Oxygen isotope fractionation between water and the aqueous hydroxide ion. *Geochim. Cosmochim. Acta* 289, 182–195
- Zeebe R. E. and Wolf-Gladrow D. A. (2001) CO<sub>2</sub> in seawater: equilibrium, kinetics, isotopes. Elsevier Oceanography Series, Amsterdam.
- Zhang J., Quay P. D. and Wilbur D. O. (1995) Carbon isotope fractionation during gas-water exchange and dissolution of CO<sub>2</sub>. *Geochim. Cosmochim. Acta* **59**, 107–114.
- Zhang H., Blanco-Ameijeiras S., Hopkinson B. M., Bernasconi S. M., Mejia L. M., Liu C. and Stoll H. (2021) An isotope label method for empirical detection of carbonic anhydrase in the calcification pathway of the coccolithophore *Emiliania huxleyi*. *Geochim. Cosmochim. Acta* 292, 78–93.
- Zhou G. T. and Zheng Y. F. (2003) An experimental study of oxygen isotope fractionation between inorganically precipitated aragonite and water at low temperatures. *Geochem. Cosmochim. Acta* 67, 387–399.